ENERGY-EFFICIENT READING OF CORRELATED WIRELESS SENSORS

A Dissertation
Presented to
The Academic Faculty

by

Alper Akanser

In Partial Fulfillment
of the Requirements for the Degree
Doctor of Philosophy in the
School of Electrical and Computer Engineering

Georgia Institute of Technology
August 2016

ENERGY-EFFICIENT READING OF CORRELATED WIRELESS SENSORS

Approved by:

Dr. Mary Ann Weitnauer, Advisor
School of Electrical and Computer Engineering
Georgia Institute of Technology

Dr. Hua Wang
School of Electrical and Computer Engineering
Georgia Institute of Technology

Dr. Gregory Durgin
School of Electrical and Computer Engineering
Georgia Institute of Technology

Dr. Randall Guensler
School of Civil and Environmental Engineering
Georgia Institute of Technology

Dr. Arthur Koblasz
School of Electrical and Computer Engineering
Georgia Institute of Technology

Date Approved: May 2nd, 2016

To my Wife, Parents, and Advisor.

ACKNOWLEDGEMENTS

I would like to thank my advisor, Dr. Mary Ann Weitnauer, for her invaluable guidance and never-ending support in the pursuit of this research. This research would not be complete if it wasn't for her efforts to listen to my research, advise me further, and motivate me at every step along the way. I will always appreciate her great role in my research.

I would also like to thank Dr. Gregory Durgin and Dr. Arthur Koblasz for providing great feedback along the way, and encouraging me in research starting from my undergraduate years. They have provided me with a great team to work with to improve the quality of my dissertation and present my research in the best way possible.

My friends and colleagues at the Smart Antenna Research Lab in addition to Transportation Engineering, too many to name individually, have also been instrumental in this research, and their help is much appreciated. I would like to specifically thank Dr. Randall Guensler from Transportation Engineering for his support in my research.

My parents, Nermin Akanser and Osman Akanser, and my sister, Ayse Akanser have always provided all the support I needed, and their continued support has enabled me to complete this research. I would like to thank them for always being their for me.

Finally, I wouldn't be here without my wife, Ozum Akanser, who has relentlessly supported and encouraged me through the whole process. Thank you love!

TABLE OF CONTENTS

LIST OF TABLES

LIST OF FIGURES

SUMMARY

The objective of this dissertation is to design and analyze data fusion schemes for energy efficient reading of correlated wireless sensors using cooperative communications. A spatially correlated sensor network is read by a collector or fusion center using the semi-cooperative spectrum fusion (SCSF) scheme, where a large number of sensors simultaneously transmit to the fusion center in response to a beacon transmission by the fusion center. The sensors use the sensed data to modulate their transmit waveforms onto a set of orthogonal diversity channels. Data fusion is done automatically in the physical layer, since the sensor signals are superimposed in the received signal at the fusion center. The SCSF scheme eliminates the overhead from data sharing between sensors and medium access control (MAC) signaling.

In this research, the SCSF scheme is considered for parameter estimation and binary integration problems. In the parameter estimation case, an analog field parameter is estimated over a field at the fusion center. The inverse normalized mean squared error (INMSE) of the estimator is analyzed for the estimated parameter. The key contribution of the research is the design of SCSF scheme considering INMSE. The main contributions of the research for the parameter estimation case are the formulation of an approximation for theoretical estimation performance, scheme simulation for various scenarios, formulation of system parameter bounds for best estimation performance and investigation of the system energy use. In the binary integration case, binary sensor decisions are transmitted and integrated at the fusion center. The key contribution of the research for the binary integration case is the exact analysis of detection performance for different communication channels under various sensor deployment scenarios in terms of the probability of detection and probability of false alarm.

CHAPTER I

INTRODUCTION

Wireless sensor networks (WSNs) are networks of energy-limited sensors that measure physical phenomena and relay data to an information sink [19, 25]. In this dissertation, the reading of correlated sensors is considered; for example, generation of a temperature contour map of a field as a function of location from wireless temperature sensors, or detection of an event from individual sensor decisions. The proposed research is to use cooperative communications, specifically semi-cooperative spectrum fusion, to read the correlated sensors. In cooperative communications, a group of sensors simultaneously transmit their signals utilizing a group of diversity channels. The goal of this research is to exploit the inherent correlation of the transmitted data by using cooperative communications. There are a large number of applications where the sensed data are correlated.

1.1 Motivation

A common event detection problem is the detection of a moving vehicle in an environment monitored by wireless sensors [32]. Consider the bridge pictured in Figure 1, where a truck is moving in an environment that is monitored by wireless sensors deployed on the bridge. In this case, the sensors make their individual decisions on the existence of the truck and transmit their decisions to the base station receiver (marked as (a) in Figure 1). Since the sensor decisions concern a common event, this is a case of correlated data.

Alternatively, wireless sensors can also be used to monitor the structural health of a bridge [35]. In this case, wireless sensors sense vibrations along with other phenomena that are correlated in space and time. After some local processing, this

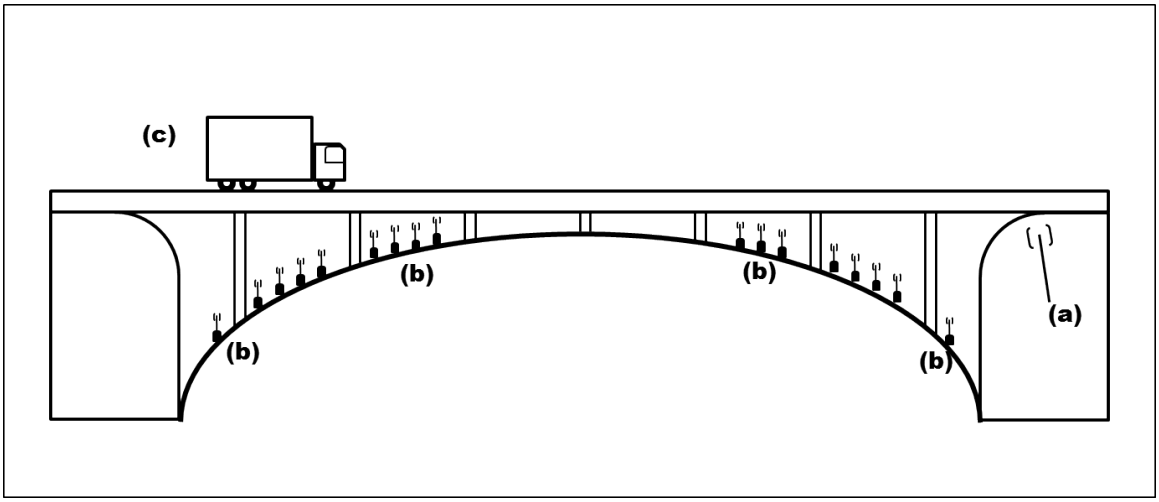

Figure 1: Wireless sensor network deployed over a bridge with base station or collector (a), individual wireless sensors (b) and a moving truck (c) shown.

data is communicated to a base station located nearby. Applications like structural health monitoring require lifetimes of years on low power modes, and cooperative schemes can aid in accomplishing such a long lifetime by exploiting the inherent correlation in the data. It's critical that the sensors have a common clock for accurate vibration analysis, since methods like modal analysis deteriorate in performance with less accurate time synchronization [30]. Time synchronization is another example for communication that involves correlated data, because the multiple sensors are trying to synchronize to a common clock making the transmissions correlated.

Cooperative communications can be employed for solving the problem of time synchronization in wireless sensors networks. The Cooperative Analog-and-Digital (CANDI) protocol uses the semi-cooperative spectrum fusion (SCSF) proposed in this research to exploit the correlation in the transmitted data to achieve network-wide time synchronization in a fast manner [63]. Experimental results along with simulations show the advantage of using cooperative communications for the time synchronization problem [63].

Another interesting application with correlated data is the fire detection problem. In fire detection, a group of wireless sensors monitor various parameters from an

area, typically a forest, to detect fire [27, 24]. The sensors can be equipped with infrared detectors in tandem with other gages to be able to detect a forest fire. If the sensors coverage areas overlap, correlated data is generated. For example, a cluster of sensors can have a specific area under observation, and individually make independent decisions on the existence of fire. This event can be modeled as generating correlated binary data.

Lastly, correlated data are also prevalent in health-care monitoring [17]. In health-care monitoring, sensors are used to track a variety of phenomena concerning patients. Wireless sensors placed in a home can be used to track accurate location of the person [59, 29, 56], where decisions from the various sensors would be correlated. Wearable sensors are used to track vital signs such as blood glucose level, blood pressure, pulse rate, electrocardiograph patterns, respiration rate and other such data [57]. Some of these vital signs will involve correlated data. With the miniaturization of the wireless sensors, they can also be implanted for gathering of biomedical data [46]. These implanted sensors will likely be involved in either passive communications [46], energy-harvesting [54], or ultra low-energy communications. Cooperative communications can benefit the system performance by allowing multiple sensors to exploit the correlated data.

1.2 Semi-Cooperative Spectrum Fusion

The objective of this dissertation is to design energy efficient cooperative communication schemes for a fusion center or collector reading a cluster of spatially correlated wireless sensors. The key contribution of the research is the semi-cooperative spectrum fusion (SCSF) scheme, which accomplishes data fusion in physical layer and avoids the use of medium access control (MAC) [3, 4].

In semi-cooperative spectrum fusion, a collector uses a beacon signal to illuminate a cluster of sensors that are sensing a common parameter or event on the field (shown

in Figure 2). The cluster of sensors transmit their sensed information simultaneously in response to the beacon, and the collector receives a superimposition of the sensor transmissions. In an estimation application, the collector estimates the value of the parameter from the received signal. In a decision application, the collector uses the received signal to make a decision about the event on the field.

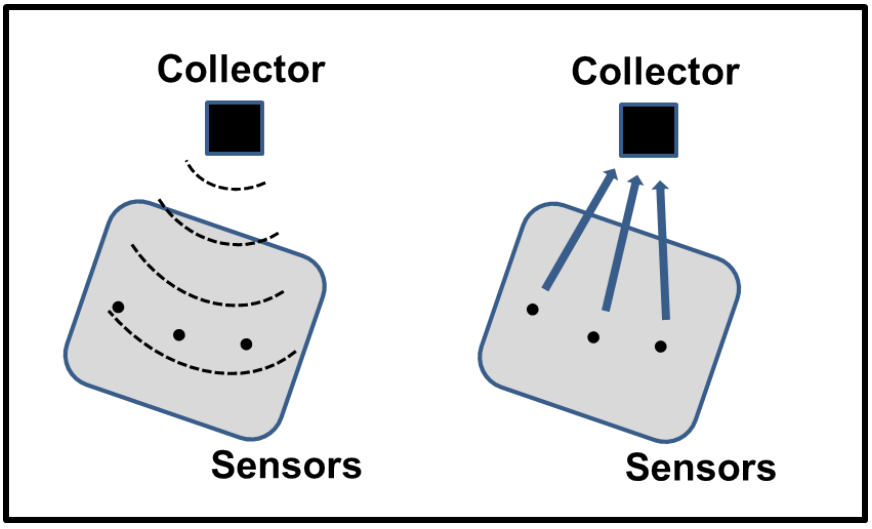

Figure 2: Semi-cooperative spectrum fusion with the beacon (left) and data response (right) phases. The sensors (shown as dots) are communicating with the collector.

In this dissertation, SCSF is designed and analyzed for parameter estimation and binary integration cases. In the parameter estimation case, a single parameter is estimated over a field with the goal of optimal inverse normalized mean squared error (INMSE) performance. In the binary integration case, binary sensor decisions are combined with the goal of optimal detection and false alarm performance. In both cases, the main contributions of this research are the theoretical analysis of the system performance in line-of-sight and fading channels in addition to the simulation of the system performance. The analysis and simulations present the performance in terms of important system parameters.

1.3 Dissertation Outline

This dissertation will present the background of the problem along with the analysis and simulation of the semi-cooperative spectrum fusion scheme. In Chapter 2, the background for data fusion and binary integration problems is presented, and the state of the art in cooperative communications and parameter estimation of harmonic processes is discussed. Chapter 2 is followed by the study of the proposed research.

The parameter estimation problem is considered in Chapter 3 with a theoretical analysis of the SCSF scheme for estimating a correlated field parameter along with simulation of the system in line-of-sight and flat fading channels. The analysis for energy expenditure is presented in Chapter 4 comparing semi-cooperative spectrum fusion with a MAC-aided protocol for the reading of a field parameter. In Chapter 5, SCSF is introduced for the binary integration problem with the theoretical analysis of the scheme for line-of-sight and flat fading channels. The contributions of this research is summarized in Chapter 6. Lastly, in Chapter 7, suggested extensions of this research are proposed.

CHAPTER II

ORIGIN AND HISTORY OF THE PROBLEM

In this chapter, a review of the state of art in data fusion, cooperative communications, and binary integration is presented in Section 2.1, Section 2.2, and Section 2.3 respectively. In addition, parameter estimation of harmonic processes is discussed in Section 2.4.

2.1 Data Fusion in Wireless Sensor Networks

When sensed information is correlated, energy can be saved using in-network data fusion after successful sensor-to-sensor communications [61, 34]. The data fusion is accomplished by applying an application-dependent data fusion algorithm to combine data from multiple sensors either at a cluster head sensor [61] or along the data relay path by successive processing at each relay sensor [34] as shown in Figure 3. In [61], the sensors randomly decide to be a cluster head and announce their id to the other sensors. During data collection, the cluster head sensors carry out data fusion after receiving all the data from the sensors in their cluster. Both of these schemes require the use of medium access control (MAC) for coordinating successful sensor-to-sensor communication.

Medium access control is also necessary for forming the sensor-clusters that are necessary for cluster-based data fusion [42]. MAC signaling causes overhead that consumes considerable energy [36]. In some environments, such as underground or on the ocean surface, sensors are not able to easily communicate with each other, making exchange of MAC and data communication signals between sensors impractical inside the network. A cooperative scheme can possibly avoid using MAC, be more energy efficient and have less delay as there is no contention for the channel. Semi-cooperative

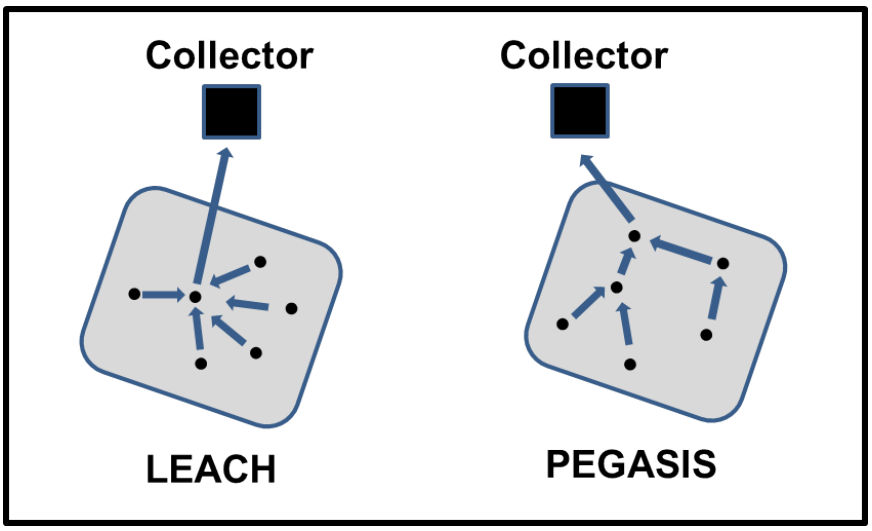

Figure 3: The flow of data in LEACH and PEGASIS data fusion protocols with the sensors shown as dots.

spectrum fusion scheme proposed in this research avoids using MAC by accomplishing data fusion in the physical layer.

2.2 Cooperative Communications in Wireless Sensors Networks

Cooperative communication is the use of a group of transmitters to transmit the same or correlated messages to a common receiver. A novel cooperative communication scheme in wireless sensor networks is the Opportunistic Large Array (OLA) [52]. The function of an OLA is to simply relay a digitally modulated signal in a wireless sensor network. A leader wireless sensor recruits other wireless sensors to transmit a common message. In other words, all the wireless sensors transmit the same message to achieve an energy efficient transmission. On the other hand, in this dissertation, the sensors using the SCSF scheme do not transmit exact same message; instead, they transmit messages that depend on sensed correlated data, which is not guaranteed to be same.

[60] and [7] consider using beacon signals from a fusion center or collector in order to initiate transmissions from wireless sensors. The reading of the wireless sensors is

accomplished by retrieving information in the modulated responses from the sensors. In [60], wireless sensors amplitude modulate their signals using their measured data. Data fusion takes place at the collector during the estimation phase, but medium access control (MAC) signals are required to separate sensor transmissions. [60] also considers sensor transmissions in a shared channel. In these shared channels, other control signals are required to establish phase synchronization between the sensors. Phase synchronization errors are also considered, and [60] indicates that the errors cause estimation performance deterioration. SCSF scheme proposed in this research uses multiple diversity channels to overcome the lack of phase synchronization. A key contribution of this research is the theoretical analysis of the estimation and detection performance under the assumption of uncorrected phase error.

In [7], sensors collectively respond to a beacon signal from an airborne collector using a shared channel. [7] presents the ML estimate of the bearing and range of the individual sensors when only one sensor is illuminated by the beacon signal. The sensors transmit their amplified observations and the collector receives the superimposed signal. When multiple sensors are illuminated, the estimated received waveform from each detected sensor are subtracted successively. Data fusion is carried out using amplitude modulation. For acceptable performance, the wireless sensors are assumed to know the channel state information and to be well-synchronized in time and frequency. The sensors are also assumed to use the optimal combining coefficients so that the signal received at the collector is the optimal unbiased estimator [7]. Errors in phase syncronization cause significant loss in estimation performance.

In [41], a discrete set of orthogonal waveforms are used to represent a discrete set of observations. The direct mapping of observations to orthogonal waveforms means that multiple sensors might transmit the same waveform if they have the same observation. Asymptotic case analysis, which looks at the case where the number of sensors grows to infinity, shows that this approach is optimal when the waveforms arrive coherently

with the same phase offset at the receiver, i.e., these waveforms are beam-formed to arrive constructively at the receiver [41]. When such phase synchronization is lacking, the performance is non-optimal, because the waveforms self-fade and have zero mean channel gain. [41] proposes solving this problem by using channel state information to establish perfect phase synchronization. In this dissertation, a combinatorial channel selection model is used to analyze theoretical performance without the need to use asymptotic assumptions. In other words, another key contribution of this research is to provide theoretical performance results for low number of sensors, which is not always a case for the asymptotic models.

In many practical applications, collecting channel state information is too costly, because it requires time and energy. [41] shows that cooperative schemes in zero mean channel gain situations have worse error performance when compared to perfectly synchronized channels. [62] uses performance simulations under phase error conditions and shows that the error performance deteriorates when phase error increases.

In [51], cooperative transmission of data is considered using waveforms that are the log-likelihood functions of the sensor observations. An expanding bandwidth is available for the transmissions. The bandwidth use grows at best in direct proportion to $N^{0.5}$ where N is the number of sensors and at worst with a rate in proportion to N. Complete phase synchronization and no fading are assumed to be able to accomplish the detection of the signal.

In other works, cooperative communication in shared multi-access channels are considered with an asymptotic analysis on distortion (error performance) bounds under resource limitations [23, 22]. The analysis indicates that using a shared multi-access channel and uncoded transmissions, i.e., sensors directly transmitting observation values, is optimal based on the assumption that phase synchronization has already been established. In this dissertation, the theoretical analysis provides performance results without the assumption of phase synchronization.

A practical example of the use of cooperative communications is the Glossy scheme [20], where constructive interference is utilized to flood a wireless sensor network. In the Glossy scheme, the same packet is simultaneously transmitted by multiple sensors using IEEE 802.15.4 symbols resulting in packet collusions, which are described as constructive interference since the receiver can still capture the packet under specific conditions. Glossy enables the rapid flooding of a network. While the channel state information is not considered; since the IEEE 802.15.4 protocol and radios are used, the training symbols transmitted are implicitly used for gathering channel state information.

2.3 Binary Integration in Sensor Networks

Binary Integration is the problem of a collector or a base station making a binary detection decision using individual binary decisions from a cluster of sensors. The conventional binary integration strategy is to communicate all sensor decisions to the collector, which indicates a detection if M out of N sensors have detected the event [50]. Variations of this strategy have been studied under distributed detection scenarios [26, 49] but no channel-based solutions have been suggested. [26, 49] consider the detection thresholds at local sensors, and also the global thresholds at the collector integrating the individual decisions. [26, 49] propose the optimal way of getting local thresholds for each sensor's local event detection and the global threshold used at the fusion center. In this dissertation, the effects of the communication channel is considered for the binary integration problem. A key contribution of this research is the theoretical analysis of the detection performance for different signal-to-noise ratios and number of available diversity channels along with various channel scenarios such as line-of-sight and fading channels.

A novel approach that also utilizes the individual sensor thresholds is the use of ranking order from individual sensor detection confidence values [12]. In this way, only

a subset of the sensors transmit their decisions, in accordance with their confidence in their decision creating time and energy efficiencies. A similar approach is to narrow down the transmission to only a single sensor, where only the most confident sensor transmits its decisions achieving even further efficiencies [44]. By lowering the number of transmissions, energy savings can be achieved.

The communication channel presents an important limiting factor in wireless sensor networks, which are often deployed to monitor or detect events in outdoor environments [55, 31]. In such applications, the sensors may be spread over an approximately two-dimensional plane, and the data collector can possibly be situated on an airborne platform on a manned or unmanned aerial vehicle. In relatively dense sensor deployments, a cluster of sensors may detect the same events. This dissertation analyzes the use of a cooperative communication scheme for binary integration of sensor decisions, in which the sensors simultaneously transmit their decisions to the single collector achieving binary integration in the physical layer.

[28] considers the detection of a random Gaussian signal embedded in additive Gaussian noise. Under communication constraints, each node amplifies and forwards sensor readings to the fusion center. The transmission channels can be orthogonal, equi-correlated, or random. [28] shows that detection performance is worse for non-orthogonal waveforms when compared to the orthogonal case. [33] considers a sensor network in which sensors are placed equi-spaced along a straight line, and the additive Gaussian noise in sensed measurements are correlated such that their covariance matrix has a regular pattern. Under perfect or near-perfect synchronization where path loss is also perfectly compensated for, the authors look at a shared channel that is used simultaneously by all sensors and compare it to parallel distinct channels that are allocated to individual sensors. The shared channel results in a smaller detection error than parallel distinct channels under power constraints.

2.4 Parameter Estimation of Harmonic Processes

In shared channels, the collectors receive a harmonic signal that contain signals from multiple transmitters. The estimation of sinusoid frequencies contained in a harmonic signal is similar to frequency synchronization in digital communications where maximum likelihood (ML) solutions make use of either data symbols or data symbol independence assumptions [40], which are not possible for analog data of frequency modulation when it lacks feedback. More general ML solutions and the Cramer-Rao bound (CRB) for estimating the individual sensor frequencies are tractable only in models with deterministic phase, amplitude and frequency [47]. In addition, these ML solutions require processing-intensive optimization search algorithms; therefore, for large time windows, [47] introduces the approximate ML solution, which is picking the largest frequency spectrum peak. Another frequency estimation algorithm developed with the assumption of a sinusoidal signal that has deterministic phase, amplitude and frequency, is the Multiple Signal Classification Algorithm (MUSIC) [15]. Frequency estimation of a complex exponential under multiplicative and additive noise, which are both real Gaussian processes, is covered in [65]. The proposed solution is the cyclic estimator which is shown to be the nonlinear least squares estimator and is equivalent to peak-picking in the frequency domain [65].

CHAPTER III

PARAMETER ESTIMATION IN CORRELATED WIRELESS SENSOR NETWORKS

In this chapter, the semi-cooperative spectrum fusion (SCSF) scheme is proposed for reading values of a parameter over a spatially-correlated field contour. SCSF is a scheme that doesn't require the use of medium access control. In this estimation problem, a group of wireless sensors measure this field parameter at various locations to transmit their data to an airborne collector acting as a base station.

In Section 3.1, the SCSF scheme and network setup are described. Next, the signal model for the received signal at the collector is presented in Section 3.2. In Section 3.3, the conditional power spectral density of the received signal is analyzed. The estimation process is outlined in Section 3.4 in addition to theoretical performance analysis of the estimators. Bounds on modulation index are presented in Section 3.5. Lastly, the performance results are presented in Section 3.6, and a summary included in Section 3.7.

3.1 Introduction

In semi-cooperative spectrum fusion, the sensors simultaneously transmit their measured parameters to an airborne collector or reader when triggered by a beacon signal from the collector. The collector uses a directive antenna for transmitting the beacon signal so that only a cluster of nodes is illuminated at any one time. Each sensor in the illuminated cluster synchronizes to the beacon signal and immediately responds by transmitting a simple sinusoidal waveform which is frequency modulated (i.e.,

frequency shifted) by the sensor's reading. The airborne collector receives a superposition of these waveforms, which resembles a Doppler spectrum [50]. The collector estimates the value of the parameter in the beam center from the measured spectrum.

SCSF was first introduced in [3] for the field parameter estimation problem with error performance simulations in a line-of-sight channel. Theoretical analysis of SCSF was introduced in [4], where the theoretical error performance was expressed in terms of critical system variables. In addition, results from Monte Carlo simulations for a line-of-sight channel were shown to be in close agreement with the theoretical results.

The network setup for SCSF can be seen in Figure 4, where the airborne collector, the ground sensors and the beam footprint of the collector beacon are shown. The aircraft is assumed to be flying parallel to the ground with speed v. The beam is assumed to be pointing directly below the aircraft. The footprint is defined by the null-to-null beam-width of the collector antenna.

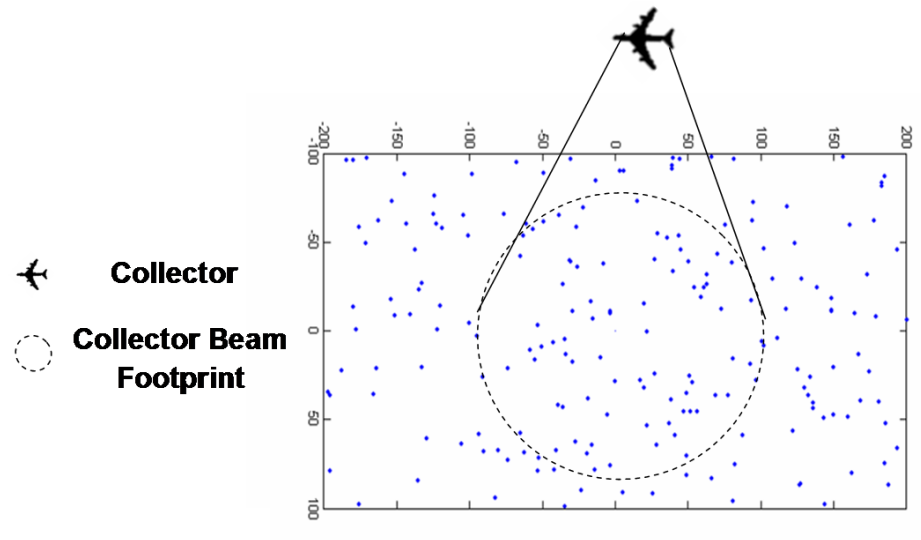

Figure 4: Sensor network setup with airborne collector flying over a field of sensors. The beam footprint is overlaid on the sensors, which are represented by small dots.

3.2 Signal Model

The sensors measure the scalar-valued field function $s(x, y)$ where (x, y) are the coordinates of a location in the field. Let $s_n = s(x_n, y_n)$ be the field value at the location of the nth sensor; then the RF frequency f'_n received from sensor n can be simply formulated as

$$f'_n = f_c + f_n + 2f_d \tag{1}$$

where f_c is the carrier frequency of the transmitted beacon, f_d is the one-way (i.e. air-to-ground or vice versa) Doppler frequency and f_n depends on the sensed information s_n according to

$$f_n = hs_n + f_o \tag{2}$$

with modulation index h and offset frequency f_o.

The sensed information, s_n, is a sample from a Gaussian distributed random field. More specifically, the sensor measurement vector $\underline{s} = [s_1, s_2, .., s_n]$ contains jointly Gaussian random variables with joint distribution $N(0, C)$. The covariance matrix C has diagonal entries of σ_s^2 and non-diagonal entries of

$$C_{ij} = \sigma_s^2 exp\left(\frac{-d_{i,j}}{r_{corr}}\right), \tag{3}$$

which depends on the distance $d_{i,j}$ between two sensors i and j and the correlation radius r_{corr}. The correlation radius is a parameter that represents the amount of spatial correlation in the field. Fields with higher values of r_{corr} have more correlation for a given distance.

An example of a deterministic field contour map is shown in Figure 5, where the z-coordinate depicts the value of the sensed parameter, whereas the x and y-coordinates refer to the field location. An airborne collector can read such a contour map by repeatedly illuminating a group of wireless sensors using SCSF. In SCSF, the illuminated wireless sensors respond simultaneously to such a beacon signal.

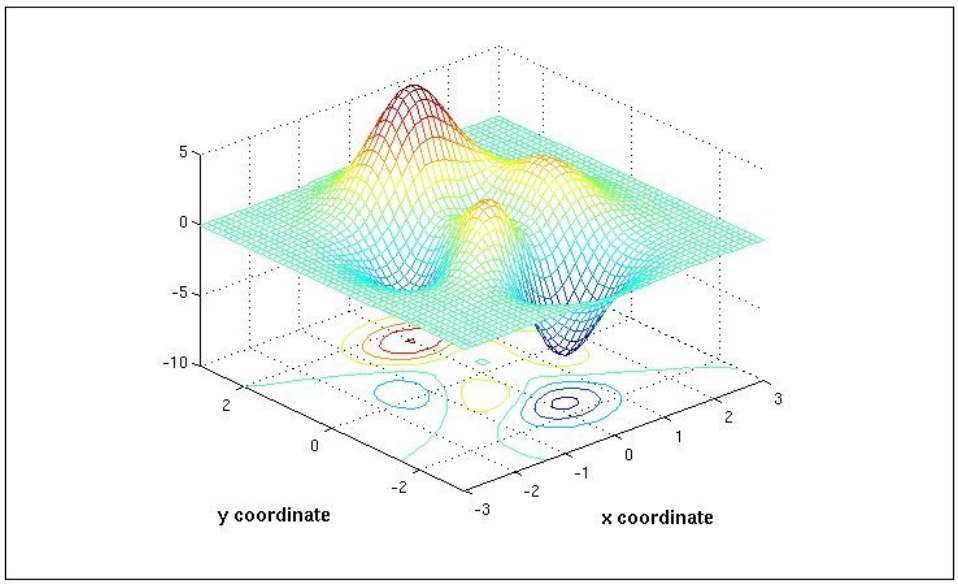

Figure 5: A deterministic field contour map showing a spatial correlation example over a 2-dimensional field (x and y-coordinates) with z-coordinate indicating the sensed value at the location.

The task of the collector, which is at an altitude of z_c as shown in Figure 6, is to estimate the field function $s_c = s(x_c, y_c)$ directly below the collector (at (x_c, y_c)) using the single reception channel output, which is the superimposition of the transmissions from multiple sensors that fall in the beam footprint.

Different estimation schemes can be employed in the SCSF approach. Two schemes considered here are the SCSF-Spectrum Mean and SCSF-MUSIC approaches. SCSF-Spectrum Mean approach estimates the spectrum as a periodogram [15], normalizes the periodogram area and then finds its mean, as though the normalized periodogram were a probability density function (PDF). SCSF-MUSIC applies the subspace-based Multiple Signal Classification (MUSIC) algorithm [15] to the received SCSF signal. These two SCSF versions are compared to the sample mean of the sensed data, which could be produced by having cluster heads poll the sensors using a MAC.

As the collector is above a sensor field, the signals go through a line-of-sight (LOS) wireless channel; therefore, the individual received amplitude from each sensor follows a simple path loss model. For the altitude of $2km$ and beamwidth of 2.5^o

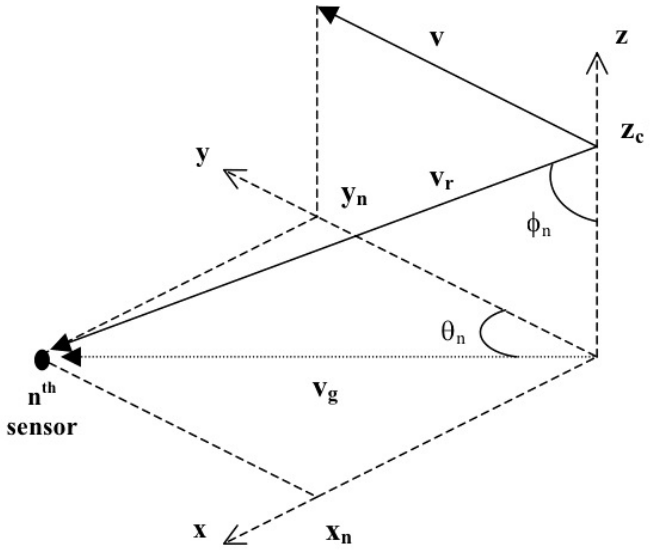

Figure 6: Collector-sensor geometry when the collector is at $(0, 0, z_c)$ and the sensor is at $(x_n, y_n, 0)$. The look down angle ϕ_n and side aspect angle θ_n depend on the geometry.

(BW) considered, the maximum variation of the path loss inside a collector footprint is less than 1%.

The collector antenna pattern response for sensor n is modeled as

$$\alpha_n = \left\{ \begin{matrix} (cos(\frac{\pi\phi_n}{BW}))^{0.5} & for\ |\frac{BW}{2}| > \phi_n \\ 0 & otherwise \end{matrix} \right\} \tag{4}$$

where ϕ_n is the collector's look-down angle for this sensor, as shown in Figure 6. Such highly directional antenna patterns are possible with the use of phased array antennas and beamformers [15] which have been widely used in aircraft of all sizes [50]. With the mentioned parameters, the model for the complex envelope $g(t)$ of the received signal at the collector, normalized by the signal level from the center of the beam center, can be expressed as

$$g(t) = \sum_{n=1}^{N} \alpha_n exp(j\Phi_n(t, f_n)) + n(t) \tag{5}$$

with

$$\Phi_n(t, f) = 2\pi(4\frac{v}{\lambda} sin\phi_n cos\theta_n t + ft - b_n), \tag{6}$$

where λ is the wavelength corresponding to the carrier frequency f_c, θ_n is the aspect angle and b_n is a uniformly distributed (between -1 and 1) random normalized phase for the n^{th} transmitting sensor. The first frequency term in (6) is the Doppler offset f_d. The random phase represents the phase responses of the sensor antennas and RF front ends, the carrier phase differences caused by the different sensor-reader distances, and intentional random phase offsets that might be inserted at the sensors. The receiver thermal noise $n(t)$ is complex additive white gaussian noise (AWGN) independent from all other parameters. For a single sensor, α, θ and ϕ all depend on the random x and y coordinates of the sensors's location.

3.3 Conditional Power Spectral Density of the Received Signal

To gain insight into the SCSF approach, it is necessary to consider the conditional power spectral density (PSD) $S_g(\nu|s_c)$ of the received signal $g(t)$ given the true value, s_c, of the field parameter in the center of the beam footprint. Assuming $\alpha_n = 1$ for all n and finite-time window effects, the PSD, conditioned on the value, s_c, of the field in the beam center, can be shown to be (detailed derivation is provided in Appendix)

$$S_g(\nu|s_c) = N \int_{\theta=-\pi}^{\pi} \int_{\phi=0}^{tan^{-1}\left(\frac{r_{ant}}{z_c}\right)} f_\theta(\theta) f_\phi(\phi) f_{s|s_c,\phi,\theta} \left(\frac{\nu - f_o - 2f_d}{h} \middle| s_c, \phi, \theta \right) d\theta d\phi + N_o. \tag{7}$$

where $f_{s|s_c,\phi,\theta}(s|s_c,\phi,\theta)$ is the conditional Gaussian PDF for the value s of the sensor field at an elevation ϕ and angle θ as described in Figure 6. The conditional PDF has mean $s_c e^{\frac{-z_c tan(\phi)}{r_{corr}}}$ and variance $\sigma_s^2 \left(1 - e^{\frac{-2z_c tan(\phi)}{r_{corr}}}\right)$.The integral is averaging over the possible values of ϕ and θ assuming that the point s is selected at random on a disc of radius r_{ant}. Therefore, θ has a uniform distribution whereas ϕ is distributed as $f_\phi(\phi) = C \tan\phi \sec\phi^2$ with constant C.

Figure 7 shows conditional PSDs for the case of $s_c = 3$ for high ($r_{corr} = 25 r_{ant}$) and low ($r_{corr} = r_{ant}$) correlation of sensed data with and without the Doppler effects. The

stem shows the frequency corresponding to the true value s_c. It is observed that the effect of Doppler spread on the conditional spectrum is negligible. Since the Doppler effect is negligible, the Doppler frequency f_d term is dropped. If $\frac{\nu - f_o}{h}$ is replaced by s in (7), then the integrand is the conditional joint PDF, $f(s, \phi, \theta | s_c)$. The result of the integral is the conditional PDF of s, given s_c. The interpretation of this conditional PDF is that it is the value of the field at some random location within the beamprint, given that the value in the center of the beamprint is s_c.

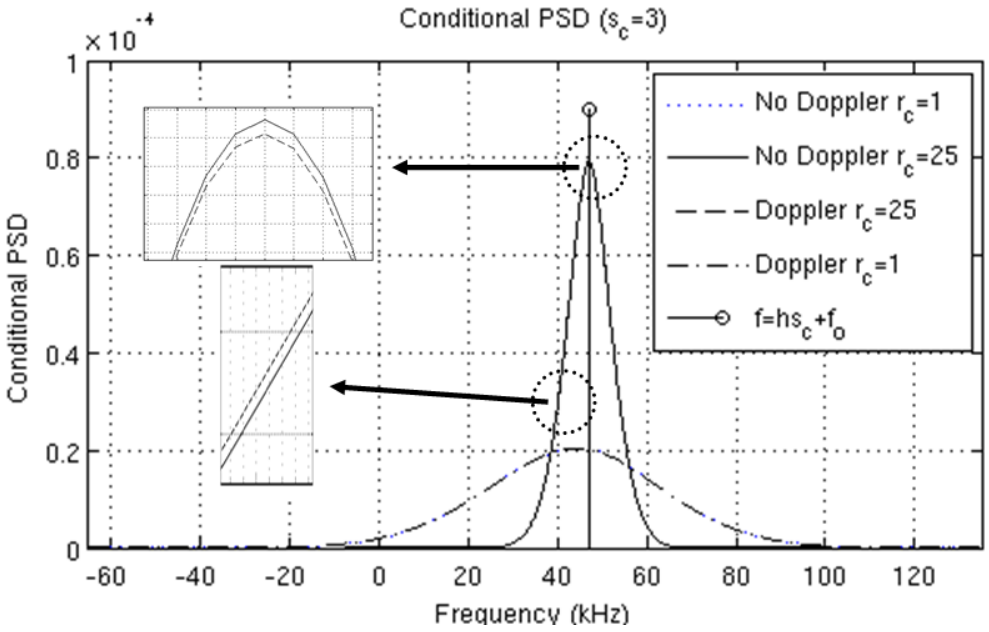

Figure 7: Conditional PSD with the s_c=3 and modulation index of 2,400, $r_c = r_{corr}/r_{ant}$ The blow-up of the peak shows the minor distinction between Doppler or Doppler-neglected conditional PSDs ($f_o = 40kHz$, z_c=2000m, N_o=0, r_{ant}=40m)

The random variable ν is defined as a simple affine function of s, $\nu = g(s) = hs + f_o$. By substituting the conditional PDF of ν into (7), the conditional PSD can be simplified to $S_g(\nu|s_c) = Nhf_\nu(\nu|s_c)$. If communication channel noise and Doppler effects are neglected, $S_g(\nu|s_c)$ can be interpreted as a scaled version of the conditional PDF of ν within the beam footprint, given only the value of the field in the beam center.

3.4 Estimation

The goal of the estimation process is to estimate the field function along the flight path at regular intervals, as shown in Figure 8. The collector estimates the field value (shown as squares in Figure 8) at the center of a circular cluster of sensors (shown as dots in Figure 8) that are illuminated by the beacon signal.

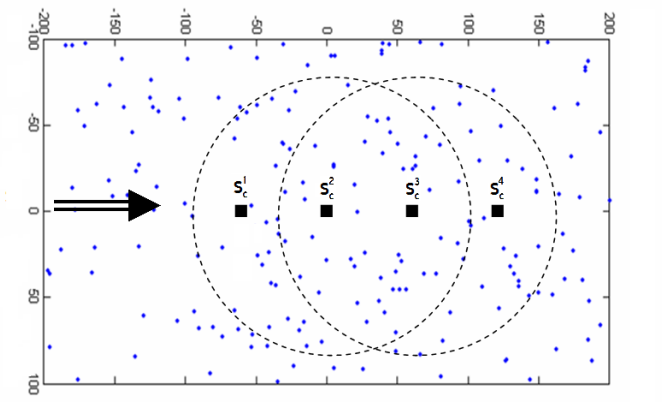

Figure 8: Sensor field including sensors (small dots), beam footprints (circlues) for the estimation of s_c^2 and s_c^3 and parameter field points at footprint centers to be estimated (squares) along with the indicated flight direction (arrow). (Not to scale)

The spatial sampling rate should be at least at the spatial Nyquist sampling rate for the field. In this section, the two semi-cooperative spectrum fusion (SCSF) estimators are introduced and compared with the sample mean estimator, which is typically used by a system with MAC. The MSE is derived for the SCSF-Spectral Mean estimator and the sample mean estimator, and bounds on modulation index for good performance are derived for the SCSF-Spectral Mean.

In the Results section, the inverse normalized mean square error (INMSE),

$$INMSE = \frac{\sigma_s^2}{MSE}, \tag{8}$$

is used to compare the estimation schemes. Normalized MSE has been used as a metric for the estimator performance [15]. When evaluating estimators, it is important to normalize the MSE, because otherwise there can be no sense of good or bad values.

For example, an MSE of $1,000$ might represent excellent performance if the range of possible values is 10^7. The INMSE can be interpreted as a signal-to-noise ratio for the field function measurement.

3.4.1 Semi-Cooperative Spectrum Fusion (SCSF) Estimators

In the two SCSF schemes, the measurement vector $\underline{s}$ is not available. Instead a superposition of the transmitted waveforms from each sensor is available. To estimate the field function $s_c = s(x_c, y_c)$ at the point (x_c, y_c) along the flight path, the collector records N_{win} samples such that the node is directly above point (x_c, y_c) midway through the window of N_{win} samples. These N_{win} samples are from the received signal that is the superposition of all the sensor signals in response to the beacon signal. The movement of the collector and beam footprint during the acquisition of the N_{win} samples is neglected in this analysis since it is small in comparison to the beam footprint radius r_{ant}, however, Doppler effects are still included in the simulation using Equation 6.

The SCSF method estimates s_c from the Discrete Fourier Transform (DFT) of the N_{win} samples. Using the k^{th} DFT frequency ν_k and k^{th} DFT value $G(k)$, the SCSF-Spectral Mean (S-SM) estimate can be formulated as

$$\hat{s}_{c,S-SM} = \frac{1}{h}\left(\frac{\sum_{k=1}^{N_{win}} \nu_k |G(k)|^2}{\sum_{k=1}^{N_{win}} |G(k)|^2} - f_o\right) \tag{9}$$

Directly analyzing the above estimator is difficult since $G(k)$ involves a superposition of sinc functions. Instead, if the Fourier Transform $G(\nu)$ is taken over an infinite time window, the estimator can be simplified as follows

$$\hat{s}_{c,S-SM} = \frac{1}{h}\left(\frac{\int_{-\infty}^{\infty} \nu |G(\nu)|^2 d\nu}{\int_{-\infty}^{\infty} |G(\nu)|^2 d\nu} - f_o\right) \tag{10}$$

where the denominator is the energy of the signal. By assuming negligible finite-time effects and Doppler effects, and a unit gain antenna pattern ($\alpha_n = 1$), and distinct sensor measurements, an approximation for the estimator becomes

$$\hat{s}_{c,S-SM} = \frac{1}{h}\left(\frac{1}{N}\int_{-\infty}^{\infty}\sum_{n=1}^{N}\nu\delta(\nu - f_n)d\nu - f_o\right) \tag{11}$$

$$\hat{s}_{c,S-SM} = \frac{1}{h}\left(\frac{1}{N}\left(\sum_{n=1}^{N} f_n\right) - f_o\right) \tag{12}$$

for high communication SNR. This is equal to the sample mean estimator (SME),

$$\hat{s}_{c,SME} = \frac{1}{N}\sum_{n=1}^{N} s_n, \tag{13}$$

therefore the sample mean estimator is an approximation for the SCSF estimator.

The SCSF-MUSIC algorithm estimates the main frequency in the time-window using the MUSIC algorithm [50] with the assumption that the window contains one complex exponential. This estimation is done separately for each window.

3.4.2 Performance of the Sample Mean Estimator (SME)

A MAC-aided network explicitly uses the vector of sensor measurements $\underline{s}$ for data fusion to calculate the Sample Mean Estimator directly. The Sample Mean Estimator is optimal in terms of Mean Squared Error when the covariance matrix C is not available [15].

The MSE for the sample mean estimator can be expressed as

$$MSE_{SME} = E\left[(\hat{s}_{c,SME} - s_c)^2\right] \tag{14}$$

$$= E[\hat{s}^2_{c,SME}] - 2E[\hat{s}_{c,SME}s_c] + E[s_c^2] \tag{15}$$

$$= \frac{1}{N^2}\sum_{n=1}^{N}\sum_{m=1}^{N} E[s_n s_m] - \frac{2}{N}\sum_{n=1}^{N} E[s_c s_n] + \sigma_s^2 \tag{16}$$

$$= \frac{1}{N^2}\sum_{n=1}^{N} E[s_n^2] + \frac{1}{N^2}\sum_{n=1}^{N}\sum_{m=1,m\neq n}^{N} E[s_n s_m] - \frac{2}{N}\sum_{n=1}^{N} E[s_c s_n] + \sigma_s^2 \tag{17}$$

To evaluate the MSE, the correlation model of (3) and intersensor distances d_{ij} are used. Since both the distances and random sensor readings s_i and s_j are identically distributed, respectively, the MSE can be further simplified to

$$\frac{MSE_{SME}}{\sigma_s^2} = \frac{N+1}{N} + \frac{N-1}{N} E_{d_{ij}}\left[e^{\frac{-d_{ij}}{r_{corr}}}\right] - 2E_{d_{ci}}\left[e^{\frac{-d_{ci}}{r_{corr}}}\right] \tag{18}$$

where the first expectation is averaging over the distances between a randomly chosen pair of sensors and the second expectation averages over the distance from the beam center to a random sensor location. The expectation in the third term simplifies to

$$E_{d_{ci}}\left[e^{\frac{-d_{ci}}{r_{corr}}}\right] = 2\left(\frac{r_{corr}}{r_{ant}}\right)^2\left(1 - \left(1 + \frac{r_{ant}}{r_{corr}}\right)e^{-\frac{r_{ant}}{r_{corr}}}\right), \tag{19}$$

whereas the expectation in the second term is evaluated through numerical integration.

3.5 Bounds on Modulation Index in Semi-Cooperative Spectrum Fusion

The value of the modulation index has an effect on the performance of the whole system. The two issues are sampling quantization errors and aliasing errors. A range of h values can be found such that these errors are small in magnitude.

3.5.1 Lower Bound (h_{min})

When the modulation index h is too-low, the implication is that the measured spectrum will not be adequately sampled. Since there are a finite number of frequency bins in the DFT, $G(k)$, there is some quantization noise in frequency points. The mean squared error that results from this quantization noise of using discrete frequency bins is expressed as

$$MSE_Q = \frac{1}{h^2}\frac{1}{12}\Delta\nu^2 = \frac{1}{12}\left(\frac{F_s}{hN_{win}}\right)^2 \tag{20}$$

in terms of frequency resolution $\Delta\nu$, sampling frequency F_s and FFT size N_{win} [48]. Assuming that the quantization noise is negligible when it is 1 order of magnitude or 10dB smaller than the sample mean estimator (SME) MSE, the lower bound becomes

$$h_{min} = \frac{F_s}{N_{win}} \sqrt{\frac{10}{12 MSE_{SME}}}, \tag{21}$$

which means that the modulation index h should be set higher than this lower bound.

3.5.2 Upper Bound (h_{max})

The upper bound for the modulation index concerns the effects of aliasing on system performance. Aliasing occurs when sensors transmit at frequencies outside the band $\frac{-F_s}{2} < \nu < \frac{F_s}{2}$. As a result of this aliasing, the frequency ν that is reported aliases to $\nu_A = \left[\left(\nu + \frac{F_s}{2}\right) \ mod \ F_s\right] - \frac{F_s}{2}$ causing an error of $\nu - \nu_A$ in the estimation process. Therefore, the MSE_A from aliasing is $\frac{1}{h^2} E\left[(\nu - \nu_A)^2\right]$ where ν is treated as a random variable whose PDF is given by the conditional power density spectrum (7). The upper bound for modulation index h_{max} is defined as the value when the MSE_A approaches one tenth of the MSE without aliasing. After plugging in the marginal distribution $f_{s_c}(s_c)$, the MSE_A is evaluated as

$$MSE_A = \frac{1}{h^2} \int_{s_c=-\infty}^{\infty} (\nu - \nu_A)^2 \, f_{s_c}(s_c) S_g(\nu | s_c) ds_c. \tag{22}$$

3.6 Results

In this section, INMSE simulation results for the MAC-free SCSF are presented in addition to the theoretical results for the sample mean estimator. Let a single trial correspond to a total of M estimates that are made along the flight path, which is path along the $x = 0$ axis in the increasing y direction for the duration of 10 milliseconds with random starting y-coordinates. The error for the mth estimate is defined as the difference of true field function (source) value s_c^m and the estimate $\hat{s}_c^m$ for that value.

Then, the MSE for the trial can be expressed as

$$MSE_{trial} = \frac{1}{M}\sum_{m=1}^{M}(s_c^m - \hat{s}_c^m)^2 \tag{23}$$

The MSE for the whole Monte Carlo experiment is averaged over a minimum of 100,000 trials using FFT size of 256 and sampling frequency of 512kHz. The footprint radius is 40m and the collector flies at a speed of 100m/s.

3.6.1 Estimation Performance

The theoretical sample mean estimator performance is expected to be a good approximation for the performance of the SCSF estimators under high communication SNR, which is defined as the ratio of average power in the superimposed signal over the average noise power. According to Equation (18), the INMSE for the sample mean estimator is expected to converge as the number of sensors per beam, N, becomes large, as shown in Figure 9 along with simulation results for the SCSF estimators in line-of-sight and Rayleigh fading channels with high communication SNR case of 30dB. The performance increases very little after $N = 10$ and exponentially before then. The approximations in the derivations are valid as the theoretical result agrees with the simulation results. As suggested by (12), the SCSF performance is approximately equal to the sample mean estimator performance. In addition, the performance in the fading environment is worse by about 0.5dB compared to the performance in the line-of-sight channel.

The main reason why the two versions of SCSF perform a little better than the sample mean estimator is because the antenna pattern gives more weight to highly correlated sensor measurements, which will be closer to the center of the beam. The SCSF-Spectral Mean performs very closely to SCSF-MUSIC algorithm, which suggests that the SCSF-Spectral Mean approach should be preferred because of its simplicity. Peak picking in the frequency domain performs at least 3dB worse in INMSE because of the higher variance in the frequency domain peak location, therefore is not

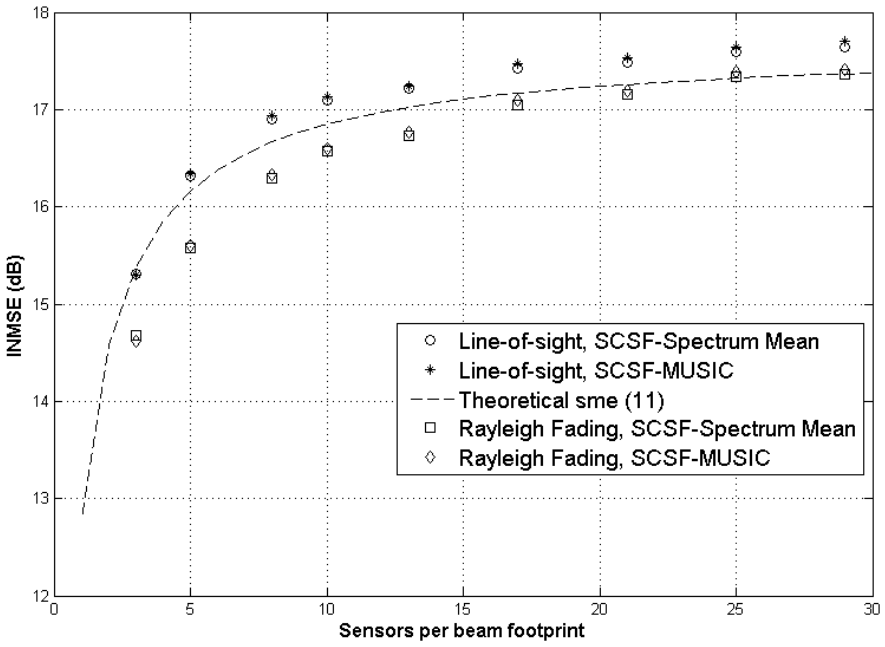

Figure 9: INMSE performance results with respect to varying sensor density for SCSF estimators in line-of-sight and Rayleigh fading channels with $r_{corr} = 25r_{ant}$, $F_s = 512kHz$, $N_{win} = 256$, $\beta = 2$. The theoretical results are shown as dashed lines.

plotted in Figure 9.

Another important parameter in Equation (18) is the correlation radius, r_{corr}. A larger correlation radius means that the sensor readings will be more correlated with the field value at the center of the beam footprint. In other words, the INMSE will be larger. According to the theoretical results, the correlation distance has an important effect on the estimation performance, which is shown in Figure 10 with the INMSE as a function of the correlation distance (in units of r_{ant}) for $N = 10$ sensors in a beam under the line-of-sight and Rayleigh fading conditions with high communication SNR.

As seen in Figure 10, INMSE increases significantly with the correlation radius, r_{corr}, as expected from the theoretical results, however the increase is gradual, and the INMSE rises above 15dB when the r_{corr} values exceed 15 times the radius of the beamprint. At $r_{corr} = 15r_{ant}$, the spatial sampling period is approximately $4r_{ant}$,

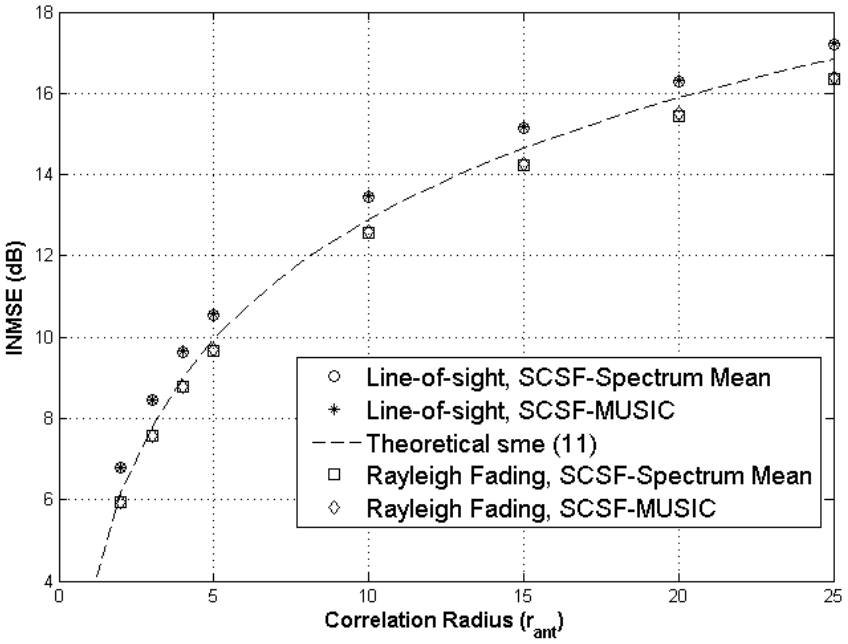

Figure 10: INMSE performance results with respect to varying degree of correlation in terms of r_{ant} for SCSF estimators in line-of-sight and Rayleigh fading channels with $N = 10,\ F_s = 1MHz,\ N_{win} = 128,\ \beta = 2$. The theoretical results are shown as dashed lines.

therefore the beam footprints do not overlap for consecutive readings. This means multiple transmissions by sensors are avoided and communication energy expenditure is reduced with respect to a lower r_{corr} level that requires overlapping.

3.6.2 Modulation Index

The INMSE performance is influenced by the modulation index according to the theoretical analysis. If the modulation index is not within the theoretical bounds derived for modulation index, namely h_{min} and h_{max} defined according to Equations 21 and 22, then the performance can noticeably degrade. These bounds are derived from the quantization and aliasing errors caused by the variation of the modulation index. These two different errors dominate for different regions of the modulation index.

The INMSE performance of the SCSF-Spectral Mean estimator with respect to

different modulation index in a line-of-sight channel with $N = 10$ under the highly correlated scenario ($r_{corr} = 25r_{ant}$) is shown in Figure 11 along with the theoretical bounds in dashed lines.

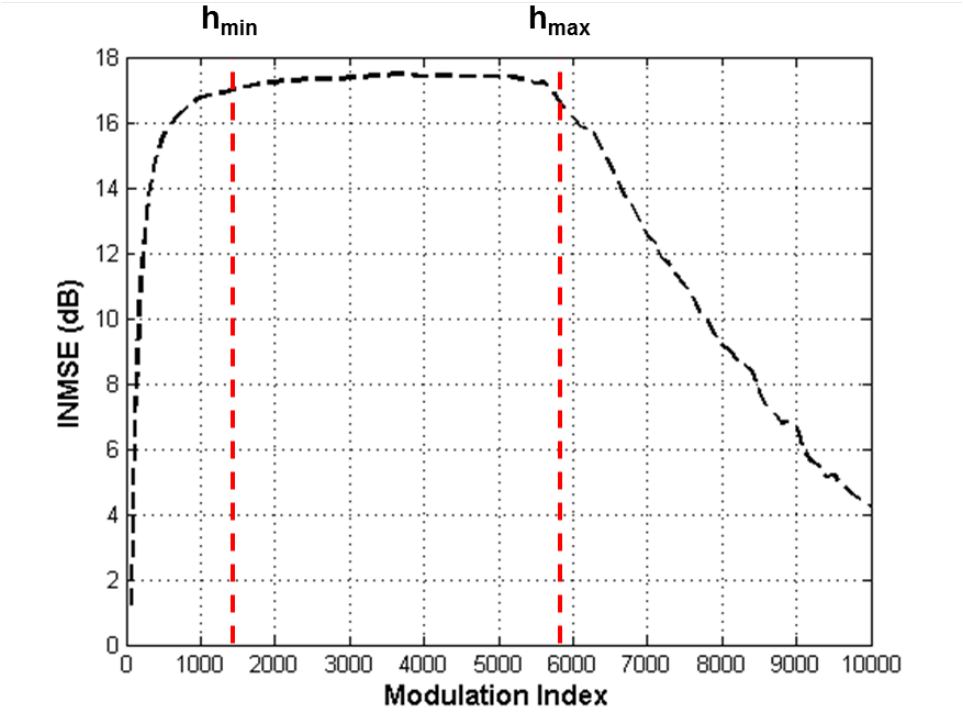

Figure 11: INMSE performance results with respect to varying different modulation index (h) for the SCSF-Spectral Mean estimator in a line-of-sight channel with $N = 10$, $F_s = 512kHz$, $N_{win} = 256$, $\beta = 2$. The theoretical bounds for h are shown as dashed lines at $h_{min} = 1.337kHz$ and $h_{max} = 5.853kHz$.

The quantization losses define the lower bound $h_{min} = 1.337kHz$ according to Equation 21, and it is a good approximate bound since the INMSE performance results become steady just after the bound as shown in Figure 11. As the modulation index increases beyond the upper bound $h_{max} = 5.853kHz$ according to Equation 22, losses due to aliasing are expected. As shown in Figure 11, the INMSE performance deteriorates around the upper bound showing that it is a good approximate bound. Both of the theoretical bounds provide a good way for the prediction of the SCSF system behavior.

The effect of the modulation index, h, on mean square error will be exponential

with respect to h in the region where the quantization noise dominates according to Equation 20, and the simulation results indicate an exponential effect for $h < h_{min}$ as shown in Figure 11. Aliasing effects dominate the mean square error for $h > h_{max}$. As shown earlier, the conditional power spectral density $S_g(\nu|s_c)$ has a h term, so the mean square error will be linear with respect to h for $h > h_{max}$ according to Equation 22. The simulation results fit the expectations from the theory for $h > h_{max}$ as seen in Figure 11.

3.7 Summary

In this chapter, the semi-cooperative spectrum fusion was introduced as a MAC-free scheme to read a field of correlated sensors. The specific parameter estimation case under consideration was a spatially correlated random Gaussian field parameter. Theoretical analysis showed that the normalized power spectral density of the signal received at the reader, assuming a long observation time and conditioned on knowing the field value in the center of this beam, is proportional to the probability density function of the beam-illuminated field value conditioned on the value in the center of the beam. With this motivation, the theoretical analysis for the sample mean estimator was presented along with results from estimation simulations in line-of-sight and Rayleigh fading channels.

The INMSE results have demonstrated that the SCSF performance is approximated by the theoretical results for the sample mean estimator. The SCSF scheme can be used to read a field of correlated wireless sensors from an aircraft flying overhead, without the use of a MAC, with an expected INMSE performance similar to the sample mean estimator. The SCSF scheme accomplishes the reading within two packet periods with the sensors transmitting simultaneously.

Lastly, the theoretical analysis included a derivation for theoretical bounds on the modulation index, which controls the transformation of sensed data to the signal

waveforms. The simulation results showed that the theoretical bounds performed well in terms of assuring SCSF INMSE performance close to the optimal INMSE performance.

CHAPTER IV

ENERGY EXPENDITURE ANALYSIS

Semi-cooperative spectrum fusion (SCSF) accomplishes data fusion in the physical layer with the goal of achieving energy savings. In this chapter, the energy expenditure is considered for parameter estimation in a wireless sensor network. The the energy expenditure is analyzed in terms of various system parameters for two different protocols: The SCSF scheme that uses no medium access control (MAC) and a conventional cluster-based LEACH scheme that uses medium access control.

4.1 Introduction

An accurate delineation of the energy expenditure of the proposed semi-cooperative spectrum fusion (SCSF) scheme with respect to other cluster-based protocols is necessary for the design and deployment of future wireless sensor networks. An important novelty of the SCSF method is the elimination of Medium Access Control (MAC), which can potentially cause energy savings. Many protocols depend on extensive use of MAC signaling even though the energy cost of the MAC is not included in previous energy comparisons of different schemes. In this chapter, energy cost model for the communication electronics of sensors in communication with an airborne receiver is presented in order to evaluate the energy comparison of SCSF vs. LEACH [61]. LEACH is a conventional cluster-based scheme that uses MAC, and it has been extensively studied in various wireless sensor network energy expenditure comparisons in the literature. The communication energy model presented here is a more advanced model than the one used in [61], which should help provide a more accurate comparison. As part of the model, firstly, the transmission and reception costs are considered, and later these costs are used to get the overall energy cost of each protocol. The

energy costs for the data processing necessary for in-network data fusion is neglected for this comparison.

4.2 Transmission and Receiving Energy Model

The energy model introduced in [61] was developed based on the Bluetooth motes [11] and the model does not fit the recent wireless sensors used in sensor networks. The current technology uses less energy for running the transmit circuitry than what is projected by the energy model in [61]. Instead, the energy costs are evaluated using the energy model put together by [13] that is based on recent research on transmitter and receiver energy-use data. In addition, the new model does a better accounting of costs involved in receiving an information packet.

In the model presented here, the main parameters are receiver sensitivity S_r, receiving power cost P_{RX}, transmitting overhead α_{TX} and reciprocal of transmitter amplifier efficiency β_{TX}. The transmitter circuitry expends P_{TX} amount of power to radiate P_{RAD} amount of power into space according to the linear dependence

$$P_{TX} = \alpha_{TX} + \beta_{TX} P_{RAD}. \tag{24}$$

For inter-sensor communication on the ground, the assumed model for power received P_{rec} at a receiver at a distance d is

$$P_{rec} = \frac{P_{RAD} G_{tr} G_r \lambda^2}{(4\pi)^2 d^3} \tag{25}$$

with transmitted power P_{RAD}, transmitter antenna gain G_{tr}, receiver antenna gain G_r and wavelength λ [48]. For a monopole antenna such as used those on a sensor, the antenna gain is equal to 1.64 [50]. When this model is written in terms of the receiver sensitivity S_r [48], the power radiated P_{RAD} to reach a distance of d can be formulated as

$$P_{RAD} = \frac{S_r (4\pi)^2}{G_{tr} G_r \lambda^2} d^3 \tag{26}$$

for intersensor communication on the ground. For reaching the airborne receiver that has a receiver with at least -111dBm sensitivity [45, 43] and around 30dB of directivity gain, a very low transmitting power available to the sensor is adequate [50]. The path loss exponent for the air-to-ground channel is 2 instead of the 3 that is used in ground-to-ground communication, since various air-to-ground measurement campaigns have found a path loss value of 2 in this case [38, 39, 37].

This energy model is used for three different transceiver units which are described in Table 1 in terms of their energy expenditure properties. These parameters are either cited directly from the technical documents provided, or estimated using other related parameters provided in the technical documents. P_{RX} is the power required by the node to run its transceiver for receiving signals.

Table 1: Energy Model Parameters for Sensor Transceivers

Transceiver	α_{TX}	β_{TX}	P_{RX}	S_r	Data Rate (R_s)	Frequency
CC2420 [58]	25 mW	0.03	35.5 mW	-94 dBm	250 kbps	2.4 GHz
Molnar [2]	0.60 mW	0.40	1.2 mW	-93 dBm	20 kbps	0.9 GHz
Otis [8]	0.25 mW	0.25	0.4 mW	-101 dBm	20 kbps	1.9 GHz

4.3 Data Fusion Protocols

In this chapter, LEACH and SCSF are described for data fusion before or during transmission to the base station or collector, i.e. the airborne receiver. LEACH is a MAC-aided cluster-based data fusion scheme, whereas SCSF is a MAC-free data fusion scheme that lets the collector beacon define the cluster by illuminating a cluster of sensors. Both of these schemes are depicted in Figure 12, where there are two different clusters that are both in communication with an airborne receiver. The dots represent the wireless sensors, and the arrows represent the flow of the data packets to the airborne receiver. LEACH does in-network data fusion by collecting all sensor data at a single wireless sensor (known as the cluster head), which transmits the fused data to the airborne receiver.

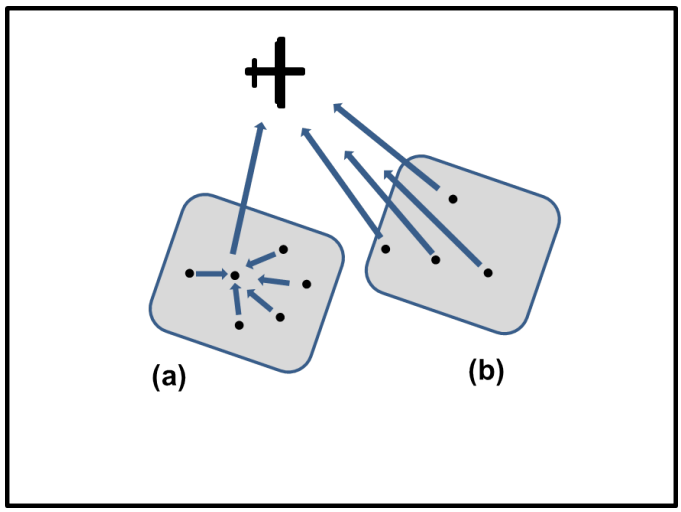

Figure 12: Two different data fusion schemes of LEACH (a) and SCSF (b) shown in two separate clusters of wireless sensors (depicted as dots) communicating with an airborne receiver.

In SCSF, all sensors receive the beacon transmission from the airborne collector, and directly transmit their data in response. The collector receives the superimposed received signal and estimates the field value. Data fusion is carried in the physical layer using SCSF without any need for MAC.

The MAC-aided cluster-based data fusion scheme LEACH consists of two phases, namely, the setup and communication phases. In the setup phase cluster heads are elected, followed by the elected cluster heads broadcasting to their clusters and all the sensors joining the cluster of the closest cluster heads. The sensors use the cluster head selection method of [61], where cluster heads are chosen randomly. In the communication phase, the sensors send their measurements to the cluster heads, which carry out data fusion and report the fused data back to the airborne receiver (the collector). The number of rounds of communication done before a new cluster head is elected is N_{setup}.

The protocol for SCSF is simpler since SCSF does not require any in-network communication. Once the sensors receive the beacon transmission from the collector, they respond simultaneously in a shared channel or a number of shared channels. The

data fusion is automatically handled by the superimposition of the various signals and the estimation or detection algorithms the collector employs.

4.4 Protocol Energy Cost

The Nyquist rate specifies the spatial sampling period as $0.25r_{corr}$ for the spatial correlation model considered. The sampling period is used to determine the number of samples (readings) N_{samp} needed for a given network. Given a square network with spatial dimensions d x d, $N_{samp} = \left(\frac{d}{0.25r_{corr}}\right)^2$. Since energy expenditure increases as the number of samples increases, the energy expenditure is inversely related to the correlation radius.

In a beam footprint with N total sensors and N_{ch} cluster heads, the following are the energy costs for the setup phase:

- Cluster heads broadcast to the clusters: N_{ch} transmissions
- Sensors receive the broadcasts: $N - N_{ch}$ receptions
- Sensors respond commitments: $N - N_{ch}$ transmissions
- Cluster heads receive commitments: $N - N_{ch}$ receptions
- Cluster heads broadcast MAC schedule: N_{ch} transmissions
- Sensors receive MAC schedule: $N - N_{ch}$ receptions

In the N_{setup} communication rounds, the energy costs are summarized as:

- Sensors receive the beacon: N receptions of header packet
- Sensors send their data: $N - N_{ch}$ transmissions consisting of header and V data samples
- Cluster heads receive: $N - N_{ch}$ receptions consisting of header and V data samples

- Cluster heads send fused data to collector: N_{ch} transmissions of header and V data samples

The headers for these packets are 4 bytes long consisting of a 1-byte-address, 1 byte of control bits and 2 bytes of syncronization information. The clusterhead broadcast packet is just the 4-byte-long header packet. The TDMA schedule broadcast packet sent by the cluster head is assumed to have a data payload of N/N_{CH} bytes in addition to the header. This payload is the transmission TDMA schedule that the sensors in the cluster follow for communication with the cluster head.

The payload for data packets in the communication phase is V data samples at 4 bytes for each data sample. The V value is dependent on the application considered but 802.15.4 has a maximum V value of about 32 [58]. The value of N_{setup} is application and hardware dependent, therefore different cases are presented in the Results section. Using this blueprint, if the N_{setup} is set sufficiently high ($N_{setup} > 50$), the setup phase energy cost is negligible and communication phase energy cost dominates. Neglecting the setup rounds and only considering the communication phase, the energy E_{MAC} spent in a network using MAC-aided cluster-based scheme can be expressed as

$$E_{MAC} = ((1+V)N_{CH}P_{TX,air}+(1+V)(N-N_{CH})P_{TX,gr}+(N+(1+V)(N-N_{CH})P_{RX})\frac{32}{R_s} \tag{27}$$

where $P_{TX,gr}$ and $P_{TX,air}$ are the transmission costs for the sensor to cluster head and the cluster head to collector communication, respectively, as formulated in (24). For $N > 10$, the N-term dominates (27) and the communication-phase energy can be simplified to

$$E_{MAC} = A_{MAC}B_{MAC}N \tag{28}$$

where $A_{MAC} = \frac{32}{R_s}P_{TX,gr}$, $B_{MAC} = 1 + V + (2 + V)\frac{P_{RX}}{P_{TX,gr}}$. The number of cluster heads N_{CH} needed to acquire N_{samp} estimates is $N_{CH} = N_{samp}$, and N_{FP} sensors

per cluster are needed in order to have the same estimation performance as a SCSF scheme with N_{FP} sensors in a footprint. As a result, the number of sensors in the MAC-aided cluster-based scheme is $N = N_{CH}N_{FP} = N_{samp}N_{FP}$.

In the SCSF scheme all the sensors receive the collector beacon and transmit back to the collector. Therefore in a collector beam footprint where there are N_{FP} sensors, there will be N_{FP} signal receptions and N_{FP} signal transmissions. The signal duration is long enough to give time for N_{win} frequency domain samples at F_s sampling frequency, which is determined by the particular transceiver studied, along with an extra 32 bits that serve as the header. The data part is repeated for V different data samples and the header is the same as the header in the MAC-aided cluster-based scheme. The energy cost for reading a network that has N_{samp} samples to read is

$$E_{SCSF} = N_{samp}N_{FP}\left(P_{RX}\frac{32}{R_s} + P_{TX,air}\left(\frac{32}{R_s} + V\frac{N_{win}}{F_s}\right)\right) \tag{29}$$

which, using $N = N_{samp}N_{FP}$, can again be simplified as

$$E_{SCSF} = A_{SCSF}B_{SCSF}N \tag{30}$$

with $A_{SCSF} = \frac{32}{R_s}P_{TX,air}$, $B_{SCSF} = \frac{P_{RX}}{P_{TX,air}} + 1 + V\frac{N_{win}R_s}{32F_s}$. The R_s and F_s values are transceiver hardware dependent whereas N_{win} is computed to satisfy (20) and (22).

Using these expressions, the energy savings ratio $\frac{E_{MAC}}{E_{SCSF}}$ of SCSF is

$$\frac{E_{MAC}}{E_{SCSF}} = \left(\frac{P_{TX,gr}}{P_{TX,air}}\right)\left(\frac{1 + V + (2+V)\frac{P_{RX}}{P_{TX,gr}}}{\frac{P_{RX}}{P_{TX,air}} + 1 + V\frac{N_{win}R_s}{32F_s}}\right) \tag{31}$$

which indicates the communication energy savings SCSF scheme will provide over the MAC-aided cluster-based scheme. Computed values for this ratio for different V are given in Section VI: Results. For large data packets, the ratio approaches to

$$\lim_{V\to\infty}\frac{E_{MAC}}{E_{SCSF}} = \left(\frac{P_{TX,gr}}{P_{TX,air}}\right)\left(\frac{1 + \frac{P_{RX}}{P_{TX,gr}}}{\frac{N_{win}R_s}{32F_s}}\right) \tag{32}$$

which is larger than one for the three transceivers considered. In other words, SCSF uses less energy than the MAC-aided cluster-based scheme. Values for this ratio are given in the next section.

4.5 Results

The energy cost of reading a whole 240m x 240m network from a collector at 2kms of altitude is calculated via simulation. The comparisons are done for the three transceiver energy models in Table 1. Two cases of field correlation are considered for simulations. In each setup, the estimation performance of the MAC-free and MAC-aided cluster-based schemes are set to be approximately equal. This is provided for by adjusting the number of cluster heads and sensors in MAC-aided scheme to equal the estimation performance of the SCSF scheme.

In Case A, High Correlation with $r_{corr} = 24r_{ant}$, the high degree of correlation corresponds to sparse reading of the field. Since the spatial reading/sampling period ($0.25r_{corr} = 6r_{ant}$) is much larger than the collector beam footprint diameter ($2r_{ant}$), the field is illuminated in non-overlapping beam footprints. Both SCSF and MAC-aided cluster-based schemes use one cluster of radius size r_{ant}=40m, therefore the parameters for the fusion protocols are $N_{samp} = 1$, N_{CH}=1, and $N = N_{FP}$.

In Case B, Low Correlation, a network with a low degree of correlation ($r_{corr} = 4r_{ant}$) is simulated. The low degree of correlation corresponds to more frequent spatial readings of the field. As the spatial sampling period is approximately r_{ant}, the beam footprints overlap about 40%. The MAC-free SCSF scheme accomplishes this by resorting to overlapping beam footprints, which hurts the energy-efficiency results for SCSF considerably, therefore $N_{samp} = 36$. The MAC-aided cluster-based scheme accomplishes the same estimation performance of MAC-free SCSF scheme by using as many clusters or cluster heads as N_{samp} in the network, therefore $N_{CH} = N_{samp}$. To match the estimation performance of the SCSF scheme, the MAC-aided cluster-based scheme needs N_{FP} sensors in each cluster, therefore the number of sensors in the network is $N = N_{CH}N_{FP}$.

The two different correlation cases are simulated using a Monte Carlo simulation with the given network setup. The total communication energy consumption for a

one-time reading of a network with number of data samples V=10 is shown in Figure 13. As expected from Equations 28 and 30, the energy costs are nearly linear with the number of sensors. It costs slightly more energy to read a network with low correlation distance, because more spatial samples are needed.

Figure 13 also includes different protocols and radios to show the contrast between them. In the legend, M50 and M5000 denotes the MAC-aided cluster-based protocol already described with N_{setup} values of 50 and 5000, respectively. For example, what appears to be the very top curve is actually the two curves corresponding to the two values of N_{setup} for the MAC-aided cluster-based protocol for the CC2420 radio. This indicates that N_{setup} plays a negligible role for the values considered. The next curve (down that is), the solid curve with no symbols, is for the MAC-free SCSF protocol for the CC2420. Therefore, it is seen that the MAC-free SCSF protocol saves about 25% of the energy of the MAC-aided cluster-based protocol.

The MAC-free SCSF protocol also saves much more energy for the experimental radios as shown in Figure 13. The experimental Otis and Molnar transceivers spend nearly 10 times less communication energy than the commercial CC2420 transceiver since the experimental transceivers are products of novel research into low-power consumption transceivers; therefore they have considerably lower communication power needs as indicated in Tables 1 and 2. In addition, increasing N_{setup} further doesn't give any noticeable energy cost reduction, i.e. the lowering of the cost is less than 1/10th of the difference between MAC-free SCSF and MAC-aided schemes.

The average values of the power consumption parameters in Equations 27 and 29, and calculated energy savings ratios assuming a specific number of data samples V are shown in Table 2 for the network setup considered and its geometry. The SCSF scheme saves energy over a MAC-aided cluster-based scheme for all the three different transceivers considered. The average savings can be approximately deduced from the ratio $\frac{E_{MAC}}{E_{SCSF}}$. The savings for the experimental Molnar and Otis receivers are greater

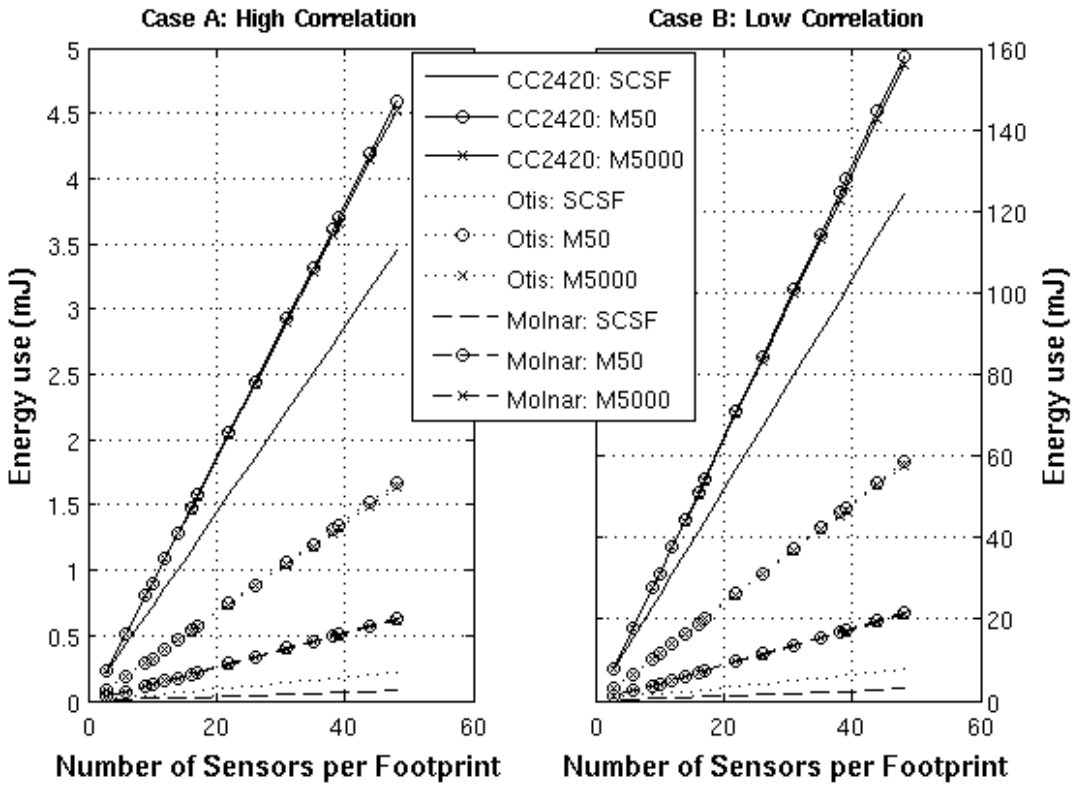

Figure 13: Energy expenditure simulation results for reading a full 240mx240m network with number of data samples V=10 using three different transceivers. (M50: MAC-aided cluster-based with N_{setup}=50, M5000: MAC-aided cluster-based with N_{setup}=5000)

because of their lower signaling rate that slows down the MAC-aided cluster-based transmit speeds and keeps the circuits on longer using up power for a longer period of time.

Table 2: Results for Energy Model Parameters and Savings Ratios

Transceiver	P_{RX}	$P_{TX,air}$	$P_{TX,gr}$	$\frac{E_{MAC}}{E_{SCSF}}$ $V=1$	$\frac{E_{MAC}}{E_{SCSF}}$ $V=10$	$\frac{E_{MAC}}{E_{SCSF}}$ $V=30$	$\frac{E_{MAC}}{E_{SCSF}}$ $V\to\infty$
CC2420 [58]	35.5 mW	25 mW	27 mW	1.49	1.33	1.30	1.11
Molnar [8]	1.20 mW	0.60 mW	0.63 mW	2.59	7.82	12.53	17.73
Otis [2]	0.40 mW	0.25 mW	0.29 mW	2.64	7.82	12.13	14.29

The Monte Carlo simulation results can also be represented as a ratio of the SCSF scheme over the MAC-aided cluster-based scheme to contrast with the numerical

values presented for these ratios in Table 2. The theoretical ratios are shown as a horizontal bound along with the simulation results for the three different transceivers with $V = 10$ and $N_{setup} = 5,000$ in Figure 14.

The energy comparison predicted in Table 2 from the simplified expressions are reflected in the actual energy cost simulation results since the energy ratios tend to the bounds with increasing numbers of sensors. In all three transceiver configurations, the MAC-free SCSF scheme uses less energy than the MAC-aided cluster-based scheme and the simulation savings show that the approximations from Table 2 are close. The energy savings ratios tend to the theoretical values calculated with increasing number of sensors because larger number of sensors was a key assumption to derive the theoretical expressions for the ratios. In addition, even for the lower number of sensors, the ratios from the simulation are close to the theoretical ratios.

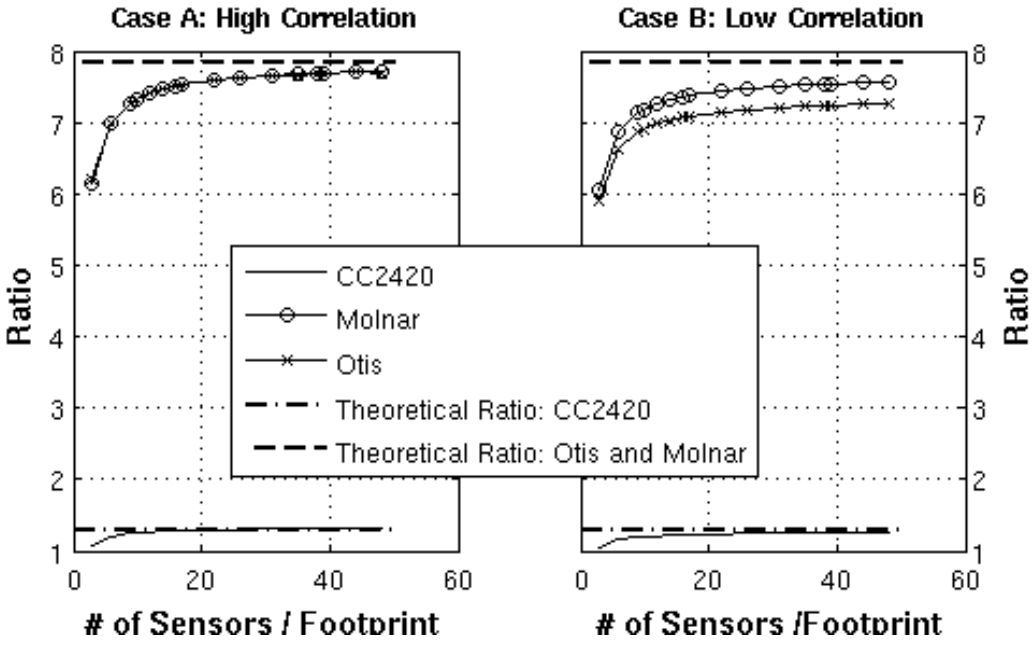

Figure 14: Energy Comparison Ratios ($\frac{E_{MAC}}{E_{SCSF}}$) with number of data samples V=10 and $N_{setup} = 5000$ using three different transceivers along with the calculated values from the theoretical ratio.

4.6 Summary

In this chapter, expressions for energy use of MAC-aided and MAC-free protocols for the reading of a correlated parameter by wireless sensors were presented along with simulations. The energy results indicate that a network using SCSF spends much less energy than a network with MAC-aided cluster-based scheme LEACH, especially for average-sized data packets. The main reasons for this difference is that the SCSF scheme avoids the numerous periods that the sensors would spend communicating with each other, and that the SCSF scheme uses cooperative communications to reach the distant airborne receiver.

The general SCSF technique is a way to read correlated parameters from any distant cluster of radios in a LOS environment. SCSF avoids the use of MAC by accomplishing data fusion in the physical layer through simultaneous wireless sensor transmissions. SCSF was shown to spend much less energy than a MAC-aided cluster-based scheme, especially for average-sized data packets.

CHAPTER V

BINARY INTEGRATION IN CORRELATED WIRELESS SENSOR NETWORKS

In this chapter, cooperative communications is considered for the binary integration problem. In Section 5.1, the binary integration problem and network setup are presented. In Section 5.2, the use of cooperative communications is proposed for binary integration. The received signal at the collector is analyzed in terms of its squared envelope in Section 5.3 for line-of-sight and flat fading channels. Lastly, Section 5.4 presents performance results, and a summary of the proposed research in binary integration is included in Section 5.5.

5.1 Introduction

Binary integration is the problem of a collector or a base station making a binary detection decision using individual binary decisions from a cluster of sensors [50]. The application considered in this work is an airborne collector in communication with a cluster of sensors on the ground as shown in Figure 15. In this setting, the sensors observe a common event but make independent binary decisions about the event. The correlation in the sensor decisions motivates the application of data fusion for the binary integration problem. In this research, cooperative communication is proposed to achieve the data fusion in this problem.

The sensor cluster can be defined as those sensors illuminated by a narrow beam from the collector. Alternatively the cluster can be defined by other means such that the collector addresses the cluster and the cluster is contained within the beam footprint of the collector. Figure 15 shows the airborne platform along with the

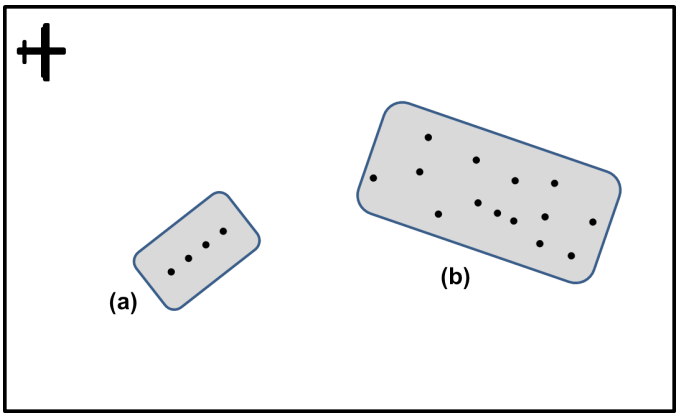

Figure 15: Binary integration problem where an airborne platform is collecting decisions from sensors (black dots) from two different clusters of sensors that are equi-distant from the collector (a) and distributed (b) in a cluster.

sensors, which are shown as solid dots organized in two separate clusters denoted as (a) and (b). The sensors in the same cluster observe a common event and each sensor makes a binary decision about this common event. In the case of cluster (a) in Figure 15, the sensors are approximately the same distance from the airborne platform and located along a line. This situation can arise if the sensors are illuminated by a beam and range-gated. In the case of cluster (b) in Figure 15, the sensors are distributed such that the distance to the airborne platform varies as a uniform random variable.

The communication channel presents an important limiting factor in wireless sensor networks, which are often deployed to monitor or detect events in outdoors environments [55, 31]. In such applications, the sensors may be spread over an approximately two-dimensional plane, and the data collector can possibly be situated on an airborne platform, which could be a manned or unmanned aerial vehicle. This chapter analyzes the use of a cooperative communication scheme for binary integration of sensor decisions, in which the sensors simultaneously transmit their decisions to the single collector achieving binary integration in the physical layer.

5.2 Cooperative Communications in Binary Integration

In relatively dense sensor deployments, a cluster of sensors may detect the same events. When the sensor decisions are correlated due to the reading application considered, energy and time efficiencies can be achieved using cooperative schemes [5]. Most of the existing solutions for reading of a field of wireless sensors require the use of medium access control (MAC) for forming sensor-clusters and coordinating wireless transmissions [14]. MAC signaling causes overhead that consumes additional time and energy, especially during the listening part of the protocols [6, 13, 58]. In addition, inter-sensor communication can be very difficult in some environments such as the ocean surface. A scheme that eliminates MAC signaling can be more practical in such environments.

A cooperative communication scheme can accomplish binary integration in two packet intervals, where the sensors *simultaneously* transmit their decisions to an airborne collector in randomly selected diversity channels. The collector triggers the transmission using a beacon transmission to illuminate a cluster of sensors, each of which responds by transmitting a waveform that is modulated by the sensor's decision onto a randomly selected diversity channel. Thus, the polling of all the sensors in the beam is completed within two packet slots, one for the beacon, and one for the superimposed responses.

If multiple sensors randomly use the same channel, their transmissions are superposed. However, this superposition is not a collision, as in a conventional network, but rather, because of diversity channels, all sensor transmissions benefit detection performance. The collector receives the transmissions in all of the channels using it for a cumulative detection decision. The sensors avoid using Medium Access Control (MAC) by randomly picking their channels. We derive the probability density function for the received squared envelope of the signal and investigate the performance of detection under this scenario.

SCSF is a scheme that does not rely on phase synchronization, and an exact analysis is presented that does not rely on asymptotic performance trends. When a number of wireless transmitters transmit in the same channel, the probability density function of the squared envelope of the phasor sum of their independent complex amplitudes is usually modeled as an exponential distribution, assuming a large number of transmitters [9, 10]. When the number of transmitters are less than 10, different probability density functions (PDFs) are necessary. Closed form expressions for the phasor sum is possible for 1 to 3 transmitters. There is no closed-form expression for cases of tranmitters larger than 3 [21, 16, 53]. However, the PDFs can still be expressed as definite integrals, and numerical computations can be achieved by using Laguerre expansion [16, 1].

In this chapter, exact PDFs are used when possible, along with the Laguerre polynomial and exponential models when applicable, to model the phasor sum. To model the use of multiple diversity channels, a combinatorial allocation of channels is considered in the analysis. The conditional PDF of the squared envelope is computed through numerical integration which is guided by the combinatorial model of diversity channel assignments. This combination of combinatorial random channel allocation and phasor sum models is novel for analysis of cooperative communication schemes and it has produced consistent results in the theoretical analysis of SCSF for binary integration. Theoretical results are also presented for Rayleigh fading channels. Lastly, the diversity gain for the SCSF scheme is shown to be evident in the probability of error.

5.3 Squared Envelope of the Received SCSF Signal

Binary integration involves N sensors that make individual decisions on whether a common event happened. Deterministic detection models, such as the sensor detection radius, have been shown to be less accurate for the sensor event detection

problem [18]. In this analysis, we use a probabilistic model for sensor detections of the event. Each sensor decides that an event happened with probability of detection P_D, given that the event happened. Similarly, each sensor decides an event happened with probability of false alarm P_{FA}, given that the event did not happen. In either case, the sensor decisions are independent from each other. A wide array of detection applications are modeled as a random process in terms of P_D and P_{FA} [18].

Given that an event has happened, the probability for N_D, the number of sensors that have decided that an event has happened ($0 \leq N_D \leq N$), is

$$P(N_D = x) = \binom{N}{x} P_D^x \left(1 - P_D\right)^{N-x}. \tag{33}$$

The goal of the SCSF scheme is to employ cooperative communication to transmit the sensor decisions to the collector. Under the SCSF scheme, a sensor that has decided on a detection transmits in one of K orthogonal channels in the detection group, whereas a sensor that has decided against a detection transmits in one of a separate set of K orthogonal channels in the non-detection group. For example, the orthogonalization can be achieved via carrier frequency, where the orthogonal channel group can be a frequency band. Alternatively, the sensors can choose from non-overlapping time slots to achieve orthogonalization. In any implementation, the sensor chooses the channel randomly out of K channels that are pre-determined to represent one of the two binary decision outcomes. The collector receives the superimposed signal, $r(t) = s(t) + w(t)$, where s(t) is the superimposition of the sensor transmissions and w(t) is the additive white Gaussian channel noise. The SNR at the receiver is defined as the ratio of average power of $s(t)$ to average power of $w(t)$. For the transmission period $0 < t < T$, the signal $s(t)$ can be expressed as

$$s(t) = \sum_{i=1}^{N_D} \sum_{k=1}^{K} \alpha_{ik}^{D} \phi_k^{D}(t) + \sum_{i=1}^{N-N_D} \sum_{k=1}^{K} \alpha_{ik}^{ND} \phi_k^{ND}(t), \tag{34}$$

where $\phi^D(t)$ and $\phi^{ND}(t)$ are the orthonormal basis functions for the communication of detection and non-detection decisions, respectively. The α^D and α^{ND} are the

projection coefficients of the received signals onto the orthonormal basis functions. After receiving the signals from the sensors, the collector makes a detection decision with cumulative probability of detection P_{CD} and cumulative probability of false alarm P_{CFA}.

In this paper, a decision statistic is computed for each of the two groups. More specifically, the decision statistic for each group is the integrated squared envelope, i.e., the L^2 norm, of the superimposed signals in the group. Because of the orthogonality of the diversity channels, $|R_D|^2$ is the sum of the squared outputs of the K matched filter receiver branches in the detection group,

$$|R_D|^2 = \sum_{k=1}^{K} |R_k|^2, \tag{35}$$

where $|R_k|^2$ is the squared envelope of the output of the k^{th} receiver branch. $|R_{ND}|^2$ is defined similarly for the non-detection group. The squared envelope from each orthogonal channel, where N_k sensors are transmitting for channel k, can be expressed as

$$|R_k|^2 = |G_k + W_k|^2, \tag{36}$$

where G_k is the sum of the complex gains from N_k sensor signals and W_k is the noise term for channel k. Given independent AWGN, the conditional PDF of $|R_k|^2$ can be expressed as

$$f_{|R_k|^2}(r|\lambda) = \frac{1}{2} e^{\frac{-r+\lambda}{2}} I_o(\sqrt{\lambda r}), \tag{37}$$

where $\lambda = |G_k|^2$ and $I_o(x)$ is the modified Bessel function of the first kind [10].

The conditional PDF for $|R_D|^2$ given N_D transmitters can be expressed as

$$f_{|R_D|^2}(r|N_D) = \sum f_{|R_D|^2}(r|N_1...N_K) P(N_1...N_K|N_D) \tag{38}$$

where the conditional PDF $f_{|R_D|^2}(r|N_1...N_K)$ is the convolution of the conditional PDFs $f_{|R_1|^2}(r|N_1)$ to $f_{|R_K|^2}(r|N_K)$, N_k is the number of transmitters in channel k $(1 \leq k \leq K)$ and the sum is over all the possible combinatorial combinations of

N_1 ... N_K given N_D with $P(N_1...N_K|N_D)$ representing the probability of the each combinatorial case. The probability for each combinatorial case can be expressed as

$$P(N_1...N_K|N_D) = \frac{N_D!}{\prod_{k=1}^{K} N_k!} \frac{1}{K^{N_D}}, \tag{39}$$

assuming each sensor chooses the orthogonal channel randomly with equal probability for each channel.

The expression of the conditional PDF for $|R_{ND}|^2$, the squared envelope of the sum of the K receiver branches in the non-detection group, follows a similar expression with the substition of $N - N_D$ instead of N_D. The collector makes its decision by comparing a threshold with the ratio of the conditional PDF of $|R_D|^2$ to the conditional PDF of $|R_{ND}|^2$.

5.3.1 Equidistant Sensors in a Line-of-sight (LOS) Channel

Each sensor's complex gain is modeled as $A'h$ where A' is the deterministic transmitter gain amplitude and h is the complex channel gain. The channel gain h is modeled as $\frac{h'}{d^\beta}$, where h' is unit amplitude for the LOS case with a random phase distributed uniformly between 0 and 2π, d is the sensor distance relative to the reference distance and β is the path loss exponent. For the case of an airborne collector focusing on a distant, small cluster in a LOS channel, the path loss differences between sensors can be negligible leading to a scenario where the sensors seem to be equidistant to the collector, i.e., d is same for all. Alternatively the sensors can originally be placed about equidistant from the receiver on a short line, also resulting in the equidistant case as shown in Figure 15.

For simplicity, a complex phasor with a random phase and deterministic amplitude $A = |A'h|$ can be used in the following theoretical expressions as d and β are assumed to be same for all sensors in the equidistant case. With these definitions, G_k becomes the sum of independent phasors, as considered in [21].

The conditional probability density function of G_k can be expressed in closed form only for $0 \leq N_k \leq 3$ [21]. For $N_k = 0$, G_k is equal to 0. For $N_k = 1$, G_k is equal to the deterministic signal amplitude A, whereas for $N_k = 2$, the probability density function of $|G_k|^2$ is expressed as

$$f_{|G_k|^2}(r|N_k = 2) = \frac{1}{\pi\sqrt{r(4A^2 - r))}}. \tag{40}$$

For the case of $N_k = 3$, the PDF of $|G_k|^2$ is expressed in terms of the elliptical integral $K(x)$ [21] as

$$f_{|G_k|^2}(r|N_k = 3) = \begin{cases} \frac{2}{\pi^2 s(r)} K(q(r)) & 0 < r < A^2 \\ \frac{2}{\pi^2 t(r)} K(q^{-1}(r)) & A^2 < r < 9A^2, \end{cases} \tag{41}$$

where the expressions $s(r)$, $t(r)$ and $q(r)$ are

$$s(r) = \sqrt{(\sqrt{r} + A)^3(3A - \sqrt{r})} \tag{42}$$

$$t(r) = 4\sqrt{A^3\sqrt{r}} \tag{43}$$

$$q(r) = \frac{t(r)}{s(r)}, \tag{44}$$

respectively. For $3 < N_k < 9$, using the Laguerre polynomial $L_m(x)$, the probability density function of $|G_k|^2$ is modeled as

$$f_{|G_k|^2}(r) = \frac{1}{N_k A^2} e^{-\frac{r}{N_k A^2}} \left(1 + \sum_{m=1}^{\infty} c_m L_m\left(\frac{r}{N_k A^2}\right)\right), \tag{45}$$

where c_m are Laguerre constants [1].

For larger N_k, $|G_k|^2$ is modeled as exponentially distributed which is the approach taken in asymptotic analysis even though it might not fit well for cases with low number of transmitters. By representing the $|G_k|^2$ more accurately for a small number of superposed transmitters, a novel non-asymptotic approach to investigating performance of cooperative communication schemes is presented in this dissertation. Using this approach, proposed research can accurately depict performance in applications where a low number of sensors are utilized.

Given the PDFs for $|G_k|^2$, the conditional PDF of $|R_k|^2$, the squared envelope in one channel with N_k transmitters, is numerically computed via Equation 37. The computed theoretical PDF is shown in Figure 16 for cases of N_k=0, 1, 2 and 5, along with PDFs computed from a simulation with 1,000,000 Monte Carlo runs for various number of transmitters in a line-of-sight channel. The path loss exponent is $\beta = 2$, since that value has been reported to be a good approximation for the ground-to-air communication channel in various experiments for a number of environment types [38, 39, 37].

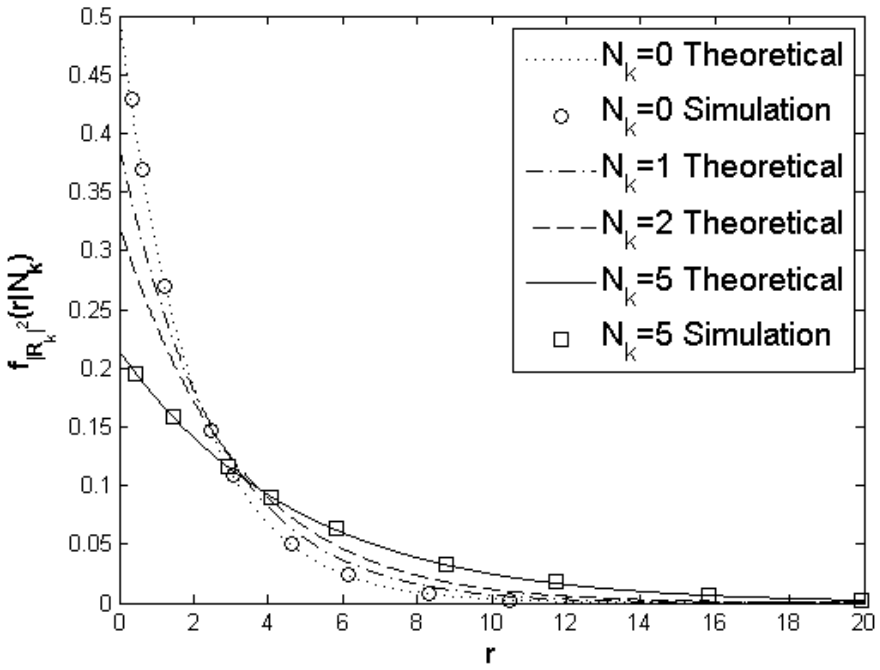

Figure 16: Conditional PDF for the squared envelope, $|R_k|^2$, of a single diversity channel with A=1 in a LOS channel for an equidistant cluster with varying number of transmitters N_k.

The values of A' and d are set such that $A = 1$ for the curves in Figure 16, because the equidistant cluster assumption assures that the sensors have the same path loss. In this particular case, the communication SNR is low meaning that the PDF is shaped by the additive white Gaussian noise. Despite the low SNR, the conditional PDFs have larger spread with increasing N_k values as more signal energy is put into

the channel with more transmitters. In addition, the theoretical PDFs show a close fit with the simulation.

The conditional PDF of $|R_D|^2$ (Equation 38) assuming each of N_D transmitters selects at random one of K orthogonal channels is shown in Figure 17 for different cases of N_D and K. A simulation with 1,000,000 Monte Carlo runs is also shown to be in close agreement with the theoretical results. For a given number of diversity channels (K), increasing the number of transmitters results in more signal energy in the group with the mean of the conditional PDF moving towards larger values of r. Likewise, for a given number of transmitters, more diversity channels results in a larger noise power also increasing the mean of $|R_D|^2$.

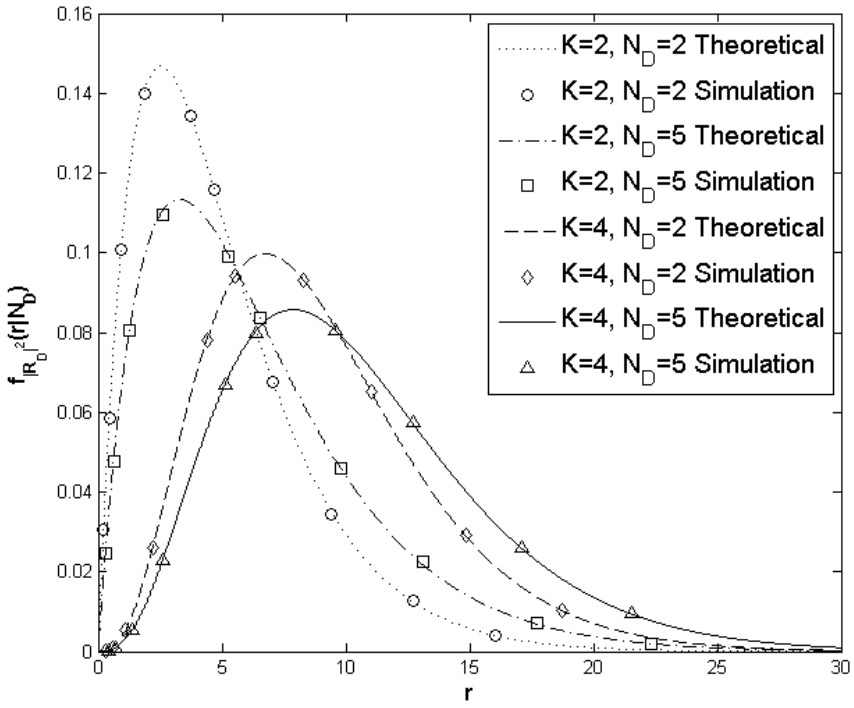

Figure 17: Conditional PDF for the squared envelope, $|R_D|^2$, of a group of diversity channels with A=1 in a LOS channel for an equidistant cluster with varying number of transmitters N_D and diversity channels K.

5.3.2 Equidistant and Distributed Sensors in a Rayleigh Fading Channel

In the Rayleigh fading channel, each sensor incurs an independently varying complex channel gain h. The gain h is modeled as $\frac{h'}{d^{\beta}}$, where h' is a complex gaussian random variable and d is a uniform random variable. As previously discussed, the equidistant case is when the sensors are equidistant from the collector as shown in Case (a) in Figure 15. In the distributed case, the sensor distances are modeled as uniform random variables corresponding to a narrow strip towards the collector as illustrated as Case (b) in Figure 15.

In the case of an equidistant group of sensors, the conditional PDF for the squared envelope $|R_k|^2$ can be computed via Equation 37. Various cases of the theoretical conditional PDF are shown in Figure 18 along with a PDF computed from a Monte Carlo simulation of equidistant transmitters in a Rayleigh fading channel.

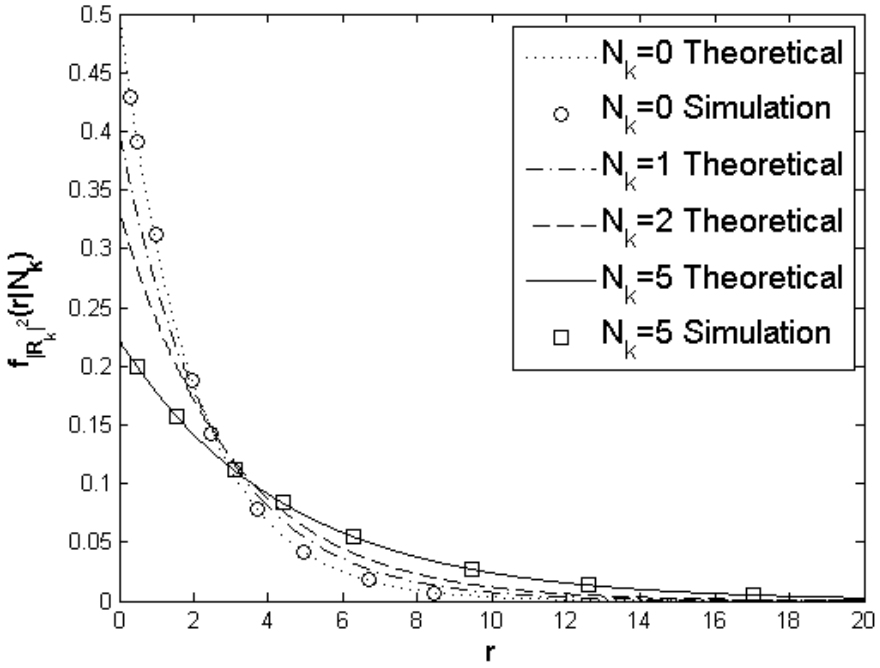

Figure 18: Conditional PDF for the squared envelope, $|R_k|^2$, of a single diversity channel in a Rayleigh fading channel for an equidistant cluster with varying number of transmitters.

The average signal power is set such that it is equivalent to the average signal power in previous LOS example (Figure 16), therefore this is also a low communication SNR case. The conditional PDFs for the squared envelope, $|R_k|^2$, of a single diversity channel with Rayleigh fading equidistant transmitters have larger spread with increasing number of transmitters as expected similar to the previous line-of-sight case. With more transmitters, more signal energy is received. In addition, the theoretical PDFs show a close fit with the simulation. Lastly, the conditional PDFs in this case are fairly similar to the conditional PDFs from the LOS case, but with slightly larger variance.

When the Rayleigh fading equidistant transmitters use a group of diversity channels, the conditional PDF of the squared envelope, $|R_D|^2$, can be computed using Equation 38 as shown in in Figure 19.

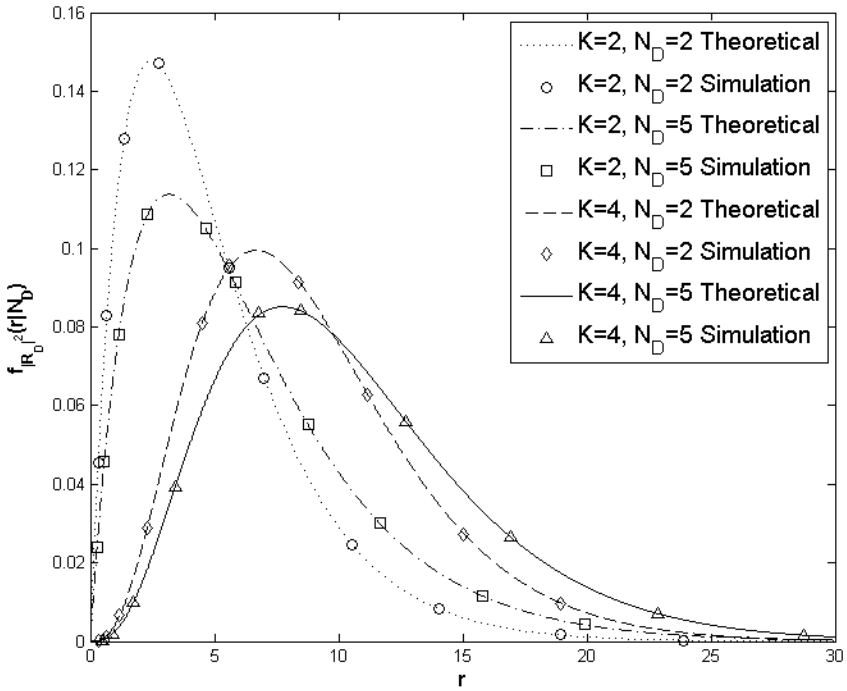

Figure 19: Conditional PDF for the squared envelope, $|R_D|^2$, of a group of diversity channels in a Rayleigh channel for an equidistant cluster with varying number of transmitters and diversity channels.

For all the different cases of number of transmitters N_D and number of diversity channels K, the conditional PDFs are fairly close to the conditional PDFs in the LOS channel, and theoretical and simulation results are in close agreement. Similar to the previous LOS case; for a given number of diversity channels (K), increasing the number of transmitters results in more signal energy in the group with the mean of the conditional PDF moving towards larger values of r. Likewise, for a given number of transmitters, more diversity channels results in a larger noise power also increasing the mean of $|R_D|^2$.

The theoretical conditional PDF for the squared envelope, $|R_k|^2$, in the case of distributed sensors shown in Figure 15 (Case (b)) can be computed via Equation 37 with the assumption of a uniform random variable for d. For the case of $1 \leq d \leq 2$, the conditional PDFs for the squared envelope, $|R_k|^2$, are shown in Figure 20 along with conditional PDFs from a Monte Carlo simulation.

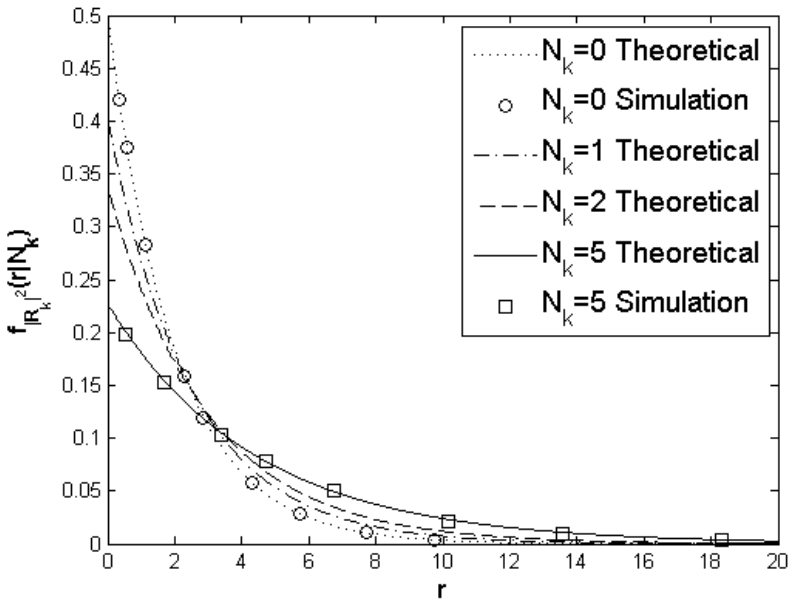

Figure 20: Conditional PDF for the squared envelope, $|R_k|^2$, of a single diversity channel in a Rayleigh fading channel for a distributed cluster with varying number of transmitters N_k.

Similar to the previous case, the N_k transmitters are Rayleigh fading transmitters.

The number of transmitters are varied as N_k=0, 1, 2 and 5 in Figure 20, and the average signal power is such that it is equal to the corresponding cases from the previous conditional PDFs shown for equidistant transmitters in line-of-sight and Rayleigh fading channels. The conditional PDFs show larger variation with increasing number of sensors and the PDFs behave similar to the LOS case hinting that the SCSF scheme can possibly exhibit similar performance behavior whether the channel is fading or not. The simulation results and theoretical results have a close fit.

Lastly, the conditional PDF of the squared envelope, $|R_D|^2$, can be computed for a distributed cluster of Rayleigh fading transmitters using Equation 38. The conditional PDFs under different cases of number of diversity channels, K, and number of transmitters, N_D, along with the simulation results are shown in Figure 21. Larger K and N_D result in larger means similar to the previous cases.

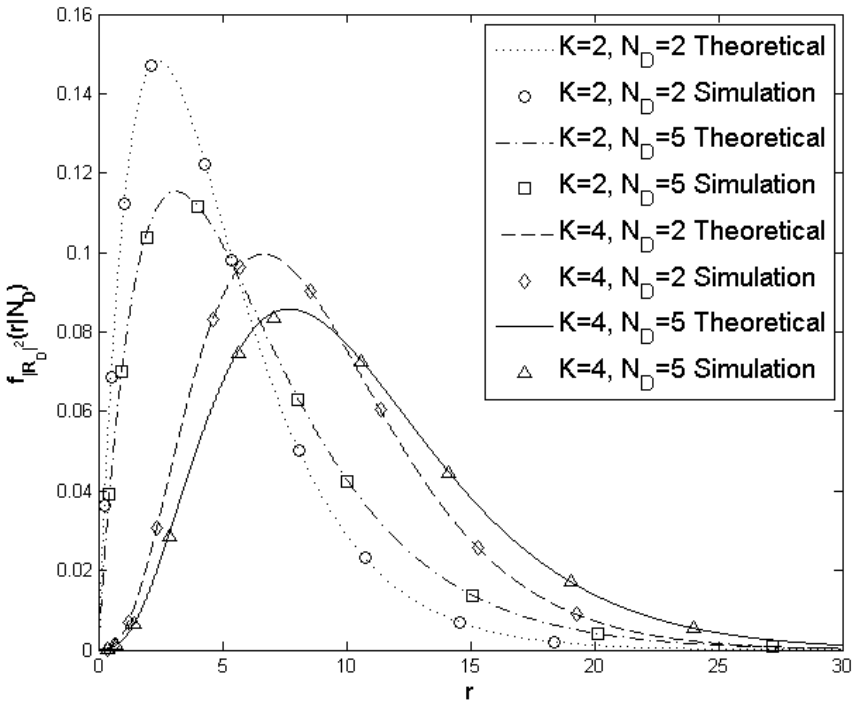

Figure 21: Conditional PDF for the squared envelope, $|R_D|^2$, of a group of diversity channels in a LOS channel for a distributed cluster with varying number of transmitters N_D and diversity channels K.

5.4 Results

In this section, results for the detection performance of the SCSF scheme for binary integration is presented by using the metrics of the cumulative detection probability, P_{CD}, and the cumulative false alarm probability, P_{CFA}, which are the probabilities at the collector for detection and false alarm respectively. The receiver operating characteristic (ROC) curve is computed to contrast the variation of P_{CD} with respect to P_{CFA} by varying the detection threshold. ROC curves for the equidistant line-of-sight case with different levels of SNR are shown in Figure 22 for $N = 20$ and $K = 2$ along with simulation results for two cases. The P_{CD} and P_{CFA} rise together with the variation of the thresholds, and simulation results agree with theoretical results. As the communication SNR increases in Figure 22, the area under the curve (AUC), which is a proxy metric for accuracy of the event detection [31], also increases, indicating performance benefits for binary integration.

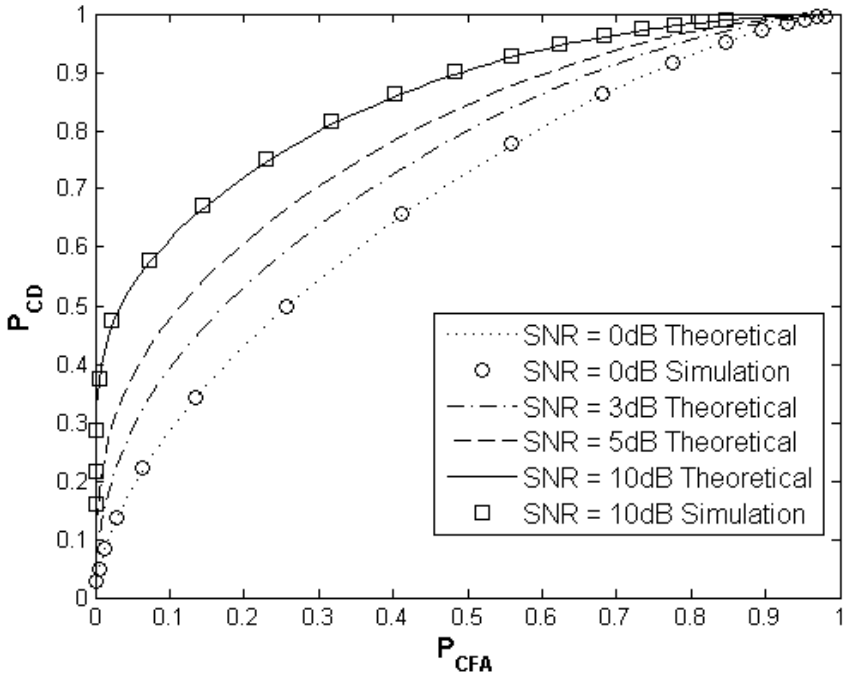

Figure 22: ROC Curve for equidistant LOS sensors under different cases of SNR with number of sensors $N = 20$ and number of diversity channels $K = 2$.

Diversity effects can be studied by keeping the SNR constant and varying the number of diversity channels K. This can be observed in Figure 23 with various ROC curves for $N = 20$. An increase in area under curve is observed as the number of orthogonal channels are increased while keeping the SNR constant. The increases are larger than in Figure 22, suggesting that increasing diversity is more effective than increasing power.

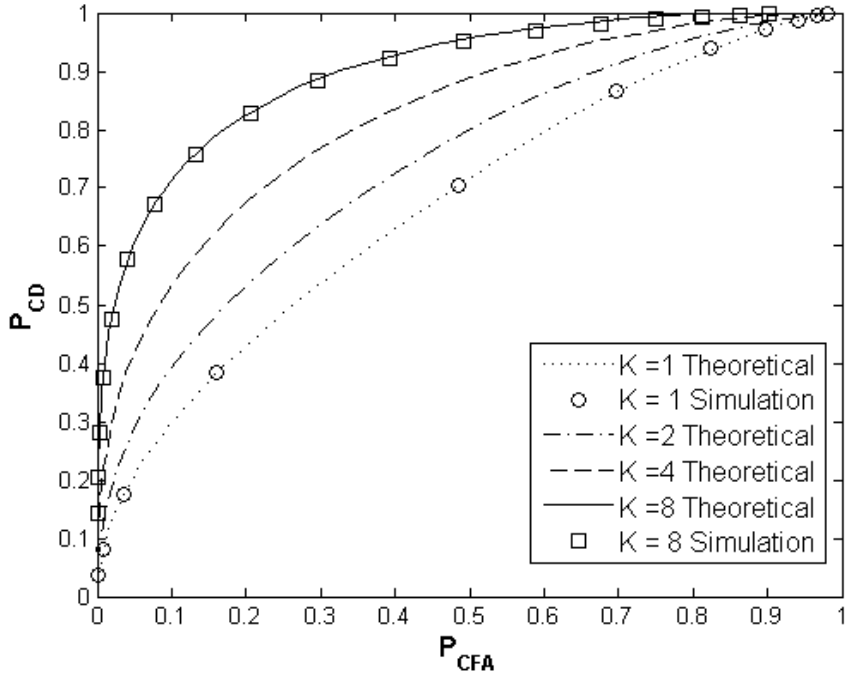

Figure 23: ROC Curve for equidistant LOS sensors under different cases of number diversity channels K with constant SNR with number of sensors $N = 20$.

When the ROC curves are computed for the Rayleigh fading channel cases with equidistant and distributed sensors, performance gains are achieved with increasing SNR, as shown in Figure 24. The path loss exponent β is 2, and the distance d uniformly varies between 1 and 2. The simulation results fit well with the theoretical results, but the former are left out of this figure due to lack of space. The performance in terms of AUC increases with increasing SNR for both kinds of sensor deployment scenarios, and performance remains close for distributed vs. equidistant scenarios.

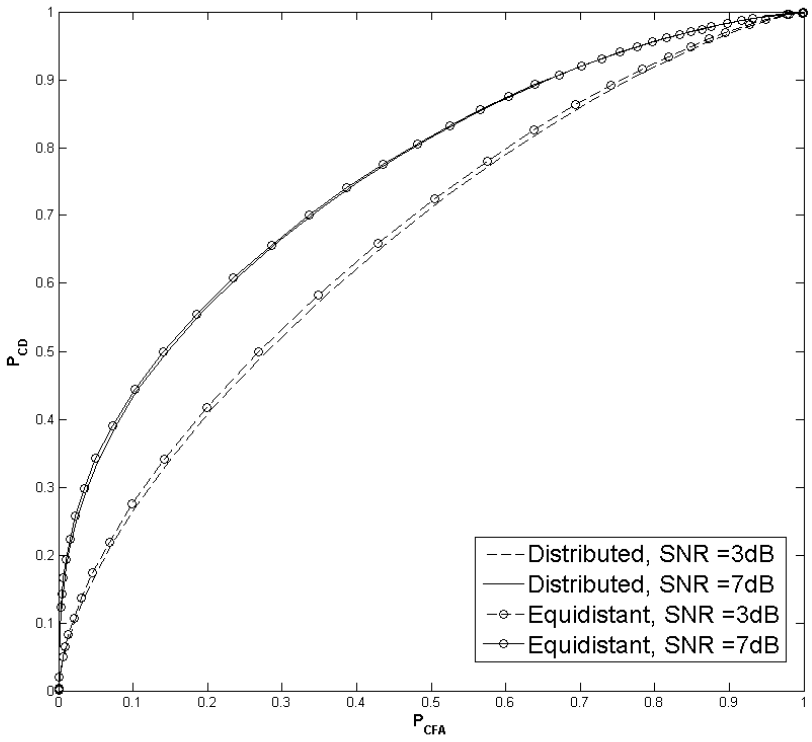

Figure 24: ROC Curve for different cases of SNR with number of sensors $N = 10$ and number of diversity channels $K = 2$ in a Rayleigh fading channel.

Under the Rayleigh fading scenario, improvements in ROC curves are observed for both equidistant and distributed cases when the number of diversity channels increases. This is shown in Figure 25 with a couple of levels of K for different deployment scenarios. The SNR is kept constant, and an increase in the area under the curve is observed.

The diversity characteristic may also be viewed in terms of the slope of the log probability curve, as it is for digital communication multiple antenna systems [64]. To achieve this, the probability of false alarm P_{CFA} is set as constant, and the SNR is varied to create a curve of probability of miss $P_M = 1 - P_{CD}$ vs. SNR using the theoretical framework presented in this paper.

The variation of the logarithm of P_M with respect to SNR in dBs for different cases

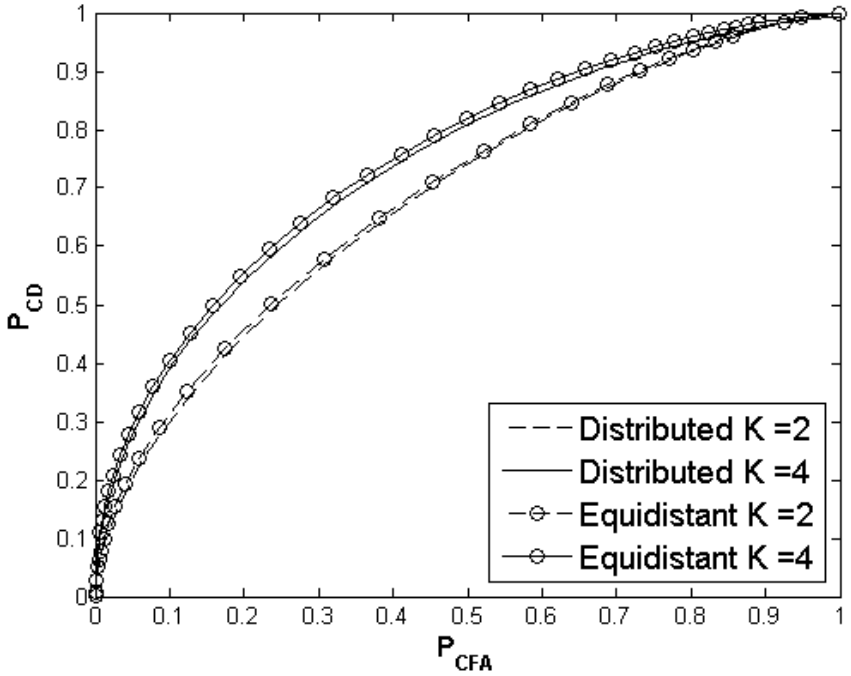

Figure 25: ROC Curve for different cases of number of diversity channels K with number of sensors $N = 10$ and constant SNR in a Rayleigh fading channel.

of diversity K=1, 2, and 4 are shown in Figure 26. In order to avoid overcrowding the figure, only the theoretical results are shown, because the simulation results are in very close agreement (i.e., like they are in previous figures for the ROC curves) with theoretical results. For each case of diversity and number of sensors ($N = 5$ and $N = 20$), results are shown for three different scenarios: equidistant sensors in a line-of-sight channel, equidistant sensors in a Rayleigh fading channel and distributed sensors in a Rayleigh fading channel.

As the number of diversity channels K increases, the slope of the performance line for each scenario increases approximately in proportion to K. In other words, better error rate reduction is achieved for the same SNR improvement, demonstrating a diversity gain. In the Rayleigh fading scenarios, adding more sensors makes a performance difference if those sensors have enough channels to utilize for diversity. This is seen in the performance results in Figure 26 as the greatest performance

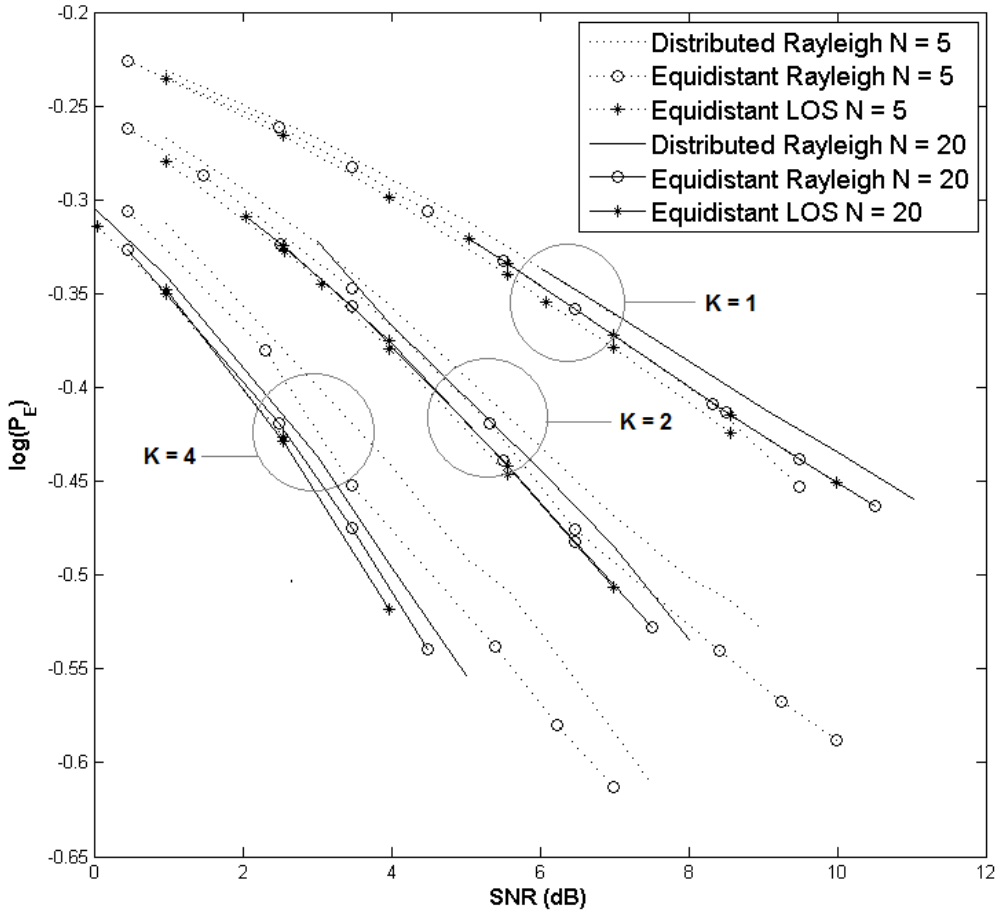

Figure 26: Probability of miss vs. SNR holding P_{CFA} constant under different diversity cases of number of diversity channels K for line-of-sight and Rayleigh channels with equidistant and distributed clusters.

difference between the cases of $N = 5$ and $N = 20$ is when the number of diversity channels K is the largest for the two Rayleigh fading scenarios.

5.5 Summary

In general, SCSF enables the polling of an arbitrarily dense deployment of sensors in just two packet intervals. This chapter addressed the case of finite number of sensors. SCSF is a novel physical layer solution to the binary integration problem. A theoretical analysis of binary integration using SCSF was presented using the exact

expressions for received signals in various channel environments for various spatial sensor distributions.

The theoretical results describe the performance of the scheme with respect to parameters concerning SNR and diversity. SCSF showed performance increases with increasing SNR and diversity as expected. The theoretical analysis also introduced a combinatorial computational approach to inspect cooperative schemes without needing to assume asymptotic conditions.

It has also been shown that SCSF achieves its main goal, which was to make use of diversity while all sensors transmitted simultaneously with no phase synchronization or medium access control. In addition to achieving this goal, diversity gains were observed indicating that the cooperative aspect of the scheme made use of the available diversity even without perfect synchronization.

CHAPTER VI

CONCLUSIONS

In this dissertation, the semi-cooperative spectrum fusion (SCSF) scheme was presented as a novel physical layer data fusion solution for the parameter estimation and binary integration problems. SCSF is a novel scheme that accomplishes data fusion in two packet intervals, avoids the use of medium access control, and requires no phase synchronization. The main contributions of this research were the design of the SCSF scheme, and the theoretical analysis of the system performance under different communication channel environments in terms of important communication channel and source data parameters.

While the contributions in this research were theoretical, the Glossy and CANDI protocols were discussed as practical implementations of either SCSF or other cooperative communication schemes. Using a similar approach, SCSF can be implemented on testbeds with off-the-shelf elements. Complete commercial implementation of SCSF will require new transceivers that can switch channels in a fast manner, but the main ideas of this research can still be considered for current implementations of cooperative communications. In the rest of this chapter, contributions and results of this research are discussed for the parameter estimation and binary integration problems.

6.1 Parameter Estimation

The proposed research involved the use of frequency shifts to represent a field parameter in order to estimate it at the collector using several different estimators. SCSF accomplished data fusion via cooperative communications.

In this dissertation, the analysis of SCSF for the parameter estimation produced

applicable system bounds, and illuminating energy use expressions. In addition, the formulation of the normalized power spectral density of the signal received at the reader, assuming a long observation time and conditioned on knowing the field value in the center of this beam, was included in this research. The spectral density has been shown to be proportional to the probability density function of the beam-illuminated field value conditioned on the value in the center of the beam.

The INMSE results for the line-of-sight and Rayleigh fading channels have shown the SCSF scheme to be competitive with the conventional scheme to read a field of correlated wireless sensors without the use of a MAC. The theoretical formulation expressed INMSE performance in terms of the number of sensors, and the correlation distance. The simulation and theoretical results matched well.

The two proposed SCSF algorithms perform closely to the alternative conventional MAC-aided network protocol in terms of INMSE. The general SCSF technique is a way to read correlated parameters from any distant cluster of wireless sensors. Lastly, SCSF was shown to spend much less energy than a MAC-aided cluster-based scheme, especially for average-sized data packets.

6.2 Binary Integration

A theoretical analysis of SCSF for the binary integration case produced results on the performance of the scheme with respect to important parameters concerning SNR and diversity. The scheme showed performance increases with increasing SNR and diversity as expected. The simulation results for detection performance agreed well with the theoretical results.

The key contribution of this research was the theoretical analysis of the detection performance for a cooperative communications scheme lacking phase synchronization without using asymptotic assumptions for the number of sensors. Another key contribution was the proposed combinatorial computational approach for the use of

diversity channels to formulate the performance of the cooperative communication schemes. Even though these contributions were made for the analysis of SCSF performance in the binary integration problem, the presented theoretical approach is applicable for the use of other cooperative communication schemes in various detection and estimation problems.

Last but not least, the main goal of the SCSF scheme was to make use of diversity while all sensors transmitted simultaneously with no phase synchronization or medium access control. This was achieved and diversity gains were observed indicating the success of the cooperative aspect of the scheme.

CHAPTER VII

SUGGESTIONS FOR FUTURE WORK

In this research, the semi-cooperative spectrum fusion scheme was considered for parameter estimation and binary integration problems. This chapter considers some of the suggestions for future work in this research area.

7.1 Parameter Estimation

A suggestion for future works is the application of the SCSF scheme to different models of parameter random processes, for example a parameter with explicit measurement error variance instead of the implicit variance introduced by the spatial correlation in this dissertation.

In addition, future works in parameter estimation using SCSF can include the use of orthogonal diversity channels instead of the analog frequency shifts. The combinatorial analysis conducted for binary integration in this dissertation can be used to analyze orthogonal diversity channels in order to have exact expressions for the estimation performance of the SCSF scheme under different scenarios of deployment, parameter variation, and communication channel models. In addition, the energy use analysis can be extended to include more aspects of the reading protocols such as processing energy costs.

7.2 Binary Integration

For the analysis of SCSF for binary integration, this research assumed that SCSF used equal numbers of diversity channels for the detection and non-detection groups for the binary integration problem. A possible topic for future work is to optimize the allocation of channels across the groups as a function of probability of detection.

Other possible next steps for this research in use of SCSF in binary integration include

1. Extension of energy model utilized in the investigation of the parameter estimation case to the binary integration case.

2. Comparison of the exact approach in this dissertation to asymptotic approaches in the literature to find out cases where asymptotic approach fails.

3. Use of the exact analysis approach for different cooperative communication schemes to study applications with low number of sensors deployed.

4. Analysis of the combining of decisions from multiple polls to improve performance.

APPENDIX A

DERIVATION OF THE CONDITIONAL POWER SPECTRAL DENSITY

Let $\underline{\mathrm{s}} = [s_1, s_2, ..., s_N]$ be the vector of field values at coordinates (x_n, y_n), and $\underline{\mathrm{x}} = [x_1, x_2, ..., x_N]$ and $\underline{\mathrm{y}} = [y_1, y_2, ..., y_N]$ be vectors of sensor x and y positions respectively, where the value s_n depends on the coordinates (x_n, y_n). The coordinates (x_n, y_n) are independent for different n. The PSD $S_g(\nu)$ of the received signal g(t) conditioned on knowing $\underline{\mathrm{s}}$, $\underline{\mathrm{x}}$, $\underline{\mathrm{y}}$ and s_c, which is the value of the field parameter in the center of the beam footprint, is formulated as

$$S_{g|s_c}(\nu|s_c, \underline{\mathrm{s}}, \underline{\mathrm{x}}, \underline{\mathrm{y}}) = \mathcal{F}\left\{R_{gg|s_c}(\tau|s_c, \underline{\mathrm{s}}, \underline{\mathrm{x}}, \underline{\mathrm{y}})\right\} \tag{46}$$

with the conditional autocorrelation $R_{gg|s_c}(\tau|s_c, \underline{\mathrm{s}}, \underline{\mathrm{x}}, \underline{\mathrm{y}})$. Here on the conditional dependence will be omitted in the subscript to prevent overcluttering of the equations. Using the independence of the complex exponential phases b_n, AWGN with energy N_o and assuming that $\alpha_n = 1$ for all n and negligible finite-time window effects, the conditional autocorrelation reduces to

$$R_{gg|s_c}(\tau|s_c, \underline{\mathrm{s}}, \underline{\mathrm{x}}, \underline{\mathrm{y}}) = E\left[g(t+\tau)g^*(\tau)\right] \tag{47}$$

$$= \sum_{n=1}^{N} e^{j2\pi(hs_n + f_o + 2f_d)\tau} + N_o\delta\left(\tau\right) \tag{48}$$

which is still a function of s_c and the random vectors $\underline{\mathrm{s}}$, $\underline{\mathrm{x}}$ and $\underline{\mathrm{y}}$. The Doppler offset f_d is a function of ϕ and θ as shown in (6), therefore also a function of x and y coordinates. The conditional PSD follows as

$$S_g(\nu|s_c, \underline{\mathrm{s}}, \underline{\mathrm{x}}, \underline{\mathrm{y}}) = \sum_{n=1}^{N} \delta\left(\nu - hs_n - f_o - 2f_d\right) + N_o. \tag{49}$$

Next the conditioning on $\underline{s}$ is removed by averaging over $\underline{s}$:

$$S_g(\nu|s_c,\underline{x},\underline{y}) = \int_{s_1} .. \int_{s_N} \sum_{n=1}^{N} \delta\left(\nu - hs_n - f_o - 2f_d\right) f_{\underline{S}}\left(\underline{s}|s_c,\underline{x},\underline{y}\right) ds_1..ds_N + N_o. \quad (50)$$

Recalling that $(s_c,\underline{s})$ is jointly Gaussian if conditioned on x_c,y_c, $\underline{x}$ and $\underline{y}$; x_c,y_c, $\underline{x}$ and $\underline{y}$ specify the autocorrelation matrix for $(s_c,\underline{s})$. Furthermore the conditional PDF of $\underline{s}$ given s_c, x_c, y_c, $\underline{x}$ and $\underline{y}$, which is denoted $f_{\underline{S}}(s|s_c,\underline{x},\underline{y})$ is also Gaussian. For the i^{th} term in the sum, it is observed that

$$\int_{s_i} \delta\left(\nu - hs_i - f_o - 2f_d\right) f_{\underline{S}}\left(\underline{s}|s_c,\underline{x},\underline{y}\right) ds_i = f_{\underline{S}}\left(s_1..s_i = \frac{\nu - f_o - 2f_d}{h}, .., s_N|s_c,\underline{x},\underline{y}\right). \quad (51)$$

Integrating the i^{th} term above (51) over the remaining s, the dependence on all s except s_i is removed as following:

$$\int_{s_1} .. \int_{s_{i-1}} \int_{s_{i+1}} .. \int_{s_N} f_{\underline{S}}\left(s_1, ..s_i = \frac{\nu - f_o - 2f_d}{h}, ..s_N|s_c,\underline{x},\underline{y}\right) ds_1 \,..\, ds_{i-1}\, ds_{i+1} \,..\, ds_N$$
$$= f_{s_i}\left(\frac{\nu - f_o - 2f_d}{h}|s_c,\underline{x},\underline{y}\right) \quad (52)$$

where $f_{s_i}\left(s_n|s_c,\underline{x},\underline{y}\right) = f_{s_i|s_c,\underline{x},\underline{y}}\left(s_n|s_c,\underline{x},\underline{y}\right)$ of s_n is the conditional PDF for s_i. Since (52) is true for all i from 1 to N, the conditional PSD becomes

$$S_g(\nu|s_c,\underline{x},\underline{y}) = \sum_{n=1}^{N} f_{s_n|s_c,x_n,y_n}\left(\frac{\nu - f_o - 2f_d}{h}\middle| s_c, x_n, y_n\right) + N_o. \quad (53)$$

Next the conditioning on $\underline{x}$ and $\underline{y}$ is removed and spherical coordinates are used by taking the expectation using the PDFs of the spherical random variables ϕ_n and θ_n

$$S_g(\nu|s_c) =$$
$$\sum_{n=1}^{N} \int_{\theta_n=-\pi}^{\pi} \int_{\phi_n=0}^{tan^{-1}\left(\frac{r_{ant}}{z_c}\right)} f_{\theta_n}(\theta_n) f_{\phi_n}(\phi_n) f_{s_n}\left(\frac{\nu - f_o - 2f_d}{h}\middle| s_c, \phi_n, \theta_n\right) d\phi_n \, d\theta_n + N_o \quad (54)$$

where θ_n are uniformly distributed and ϕ_n are distributed as $f_{\phi_n}(\phi_n) = C \tan\phi_n \sec{\phi_n}^2$ with constant C and z_c is the altitude. The conditional Gaussianity of $f_{s_n}\left(s_n|s_c,\phi_n,\theta_n\right)$

is ensured since ϕ_n and θ_n specift x_n and y_n for a given z_c. Since θ_n are identically distributed and ϕ_n are identically distributed, the sum over n can be collapsed:

$$S_g(\nu|s_c) =$$
$$N \int_{\theta=-\pi}^{\pi} \int_{\phi=0}^{tan^{-1}\left(\frac{r_{ant}}{z_c}\right)} f_\theta(\theta) f_\phi(\phi) f_{s|s_c,\phi,\theta} \left(\frac{\nu - f_o - 2f_d}{h} \middle| s_c, \phi, \theta \right) d\theta d\phi + N_o. \quad (55)$$

The conditional PDF $f_{s|s_c,\phi,\theta}$ has mean $s_c e^{\frac{-z_c tan(\phi)}{r_{corr}}}$ and variance $\sigma_s^2 \left(1 - e^{\frac{-2z_c tan(\phi)}{r_{corr}}}\right)$.

REFERENCES

[1] A. Abdi, A. H. H. and Nader-Esfahani, S., "On the pdf of the sum of random vectors," *IEEE Transactions on Communications*, vol. 48, pp. 7–12, Jan. 2000.

[2] A. Molnar, B. Lu, S. L. B. C. and Pister, K., "An ultra-low power 900 mhz rf transceiver for wireless sensor networks," IEEE Custom Integrated Circuits Conference, 2004.

[3] Akanser, A. and Ingram, M., "Mac-free reading of a network of correlated sensors," Military Communications Conference, 2007.

[4] Akanser, A. and Ingram, M., "Semi-cooperative spectrum fusion (scsf) for aerial reading of a correlated sensor field," IEEE Wireless VITAE Conference, 2009.

[5] Ammari, H., *The Art of Wireless Sensor Networks*. New York: Springer, 2013.

[6] Ammer, J. and Rabaey, J., "The energy-per-useful-bit metric for evaluating and optimizing sensor network physical layers," IEEE International Workshop on Wireless Ad Hoc and Sensor Networks, 2006.

[7] Ananthasubramaniam, B. and Madhow, U., "On localization performance in imaging sensor nets," *IEEE Transactions on Signal Processing*, vol. 55, pp. 5044–5057, Oct. 2007.

[8] B. Otis, Y. H. C. and Rabaey, J., "A 400μw rx, 1.6mw tx super-regenerative transceiver for wireless sensor networks," Symposium on VLSI Circuits, 2004.

[9] Beckmann, P., "Statistical distribution of the amplitude and phase of a multiply scattered field," *Journal of Research of the National Bureau of Standards*, vol. 66D, pp. 231–240, May 1962.

[10] Beckmann, P., *Probability in communication engineering*. San Diego, CA: Harcourt, Brace & World, 1967.

[11] Bluetooth, "Bluetooth technical information homepage," The Official Bluetooth Technology Info Site, Bluetooth SIG Inc., 2009 [Online] Available:http://www.bluetooth.com [Accessed: Aug. 4 2009].

[12] Blum, R. S. and Sadler, B. M., "Energy efficient signal detection in sensor networks using ordered transmissions," *IEEE Transactions in Signal Processing*, vol. 56, pp. 3229–3235, July 2008.

[13] B.W. Cook, S. L. and Pister, K. J., "Soc issues for rf smart dust," *Proceedings of the IEEE*, vol. 94, pp. 1177–1196, June 2006.

[14] Cecilio, J. and Furtado, P., *Wireless Sensors in Industrial Time-Critical Environments*. Zurich, Switzerland: Springer-Verlag, 2014.

[15] D. G. Manolakis, V. K. I. and Kohon, S. M., *Statistical and Adaptive Signal Processing*. New York, NY: McGraw-Hill Higher Education, 2000.

[16] Daba, J. and Bell, M., "Statistics of the scattering cross-section of a small number of random scatterers," *IEEE Transactions on Antennas and Propagation*, vol. 43, pp. 773–783, Aug. 1995.

[17] Darwish, A. and Hassanien, A. E., "Wearable and implantable wireless sensor network solutions for healthcare monitoring," *Sensors*, vol. 11, pp. 5561–5595, Oct. 2011.

[18] Duarte, M. F. and Hu, Y. H., "Vehicle classification in distributed sensor networks," *Journal of Parallel and Distributed Computing*, vol. 64, pp. 826–838, July 2004.

[19] E. Gaura, M. Allen, L. G. J. B. and Challen, G., *Wireless sensor networks: Deployments and design frameworks*. New York: Springer Science and Business Media, 2010.

[20] F. Ferrari, M. Zimmerling, L. T. and Saukh, O., "Efficient network flooding and time synchronization with glossy," Information Processing in Sensor Networks (IPSN), 2011.

[21] G. D. Durgin, T. S. R. and Wolf, D. A. D., "'new analytical models and probability density functions for fading in wireless communications," *IEEE Transactions on Communications*, vol. 50, pp. 1005–1015, June 2002.

[22] Gastpar, M., "Uncoded transmission is exactly optimal for a simple gaussian sensor network," *IEEE Transactions on Signal Processing*, vol. 54, pp. 5247–5251, Nov. 2008.

[23] Gastpar, M. and Vetterli, M., "Power, spatio-temporal bandwidth, and distortion in large sensor networks," *Journal on Selected Areas in Communications*, vol. 23, pp. 745–754, Apr. 2005.

[24] Hefeeda, M. and Bagheri, M., "Wireless sensor networks for early detection of forest fires," IEEE International Conference on Mobile Adhoc and Sensor Systems, 2007.

[25] I. F. Akyildiz, W. Su, Y. S. and Cayirci, E., "Wireless sensor networks: a survey," *Computer networks*, vol. 38, pp. 393–422, Mar. 2002.

[26] J. Han, P. K. V. and Srinivasan, R., "'distributed binary integration," *Transactions on Aerospace and Electronic Systems*, vol. 29, pp. 2–8, Jan. 1993.

[27] J. Lloret, M. Garcia, D. B. and Sendra, S., "A wireless sensor network deployment for rural and forest fire detection and verification," *Sensors*, vol. 9, pp. 8722–8747, Oct. 2009.

[28] Jayaweera, S., "Bayesian fusion performance and system optimization for distributed stochastic gaussian signal detection under communication constraints," *IEEE Transactions on Signal Processing*, vol. 55, pp. 1238–1250, Apr. 2007.

[29] J.L. Honorato, I. S. and Torres-Torriti, M., "Human detection using thermopiles," IEEE Latin American Robotic Symposium, 2008.

[30] J.P. Lynch, Y. Wang, K. L. J. Y. and Yun, C., "Performance monitoring of the geumdang bridge using a dense network of high-resolution wireless sensors," *Smart Materials and Structures*, vol. 15, p. 1561, Oct. 2006.

[31] Klein, L., *Sensor and data fusion: A tool for information assessment and decision making*. Bellingham, WA: Spie Press, 2004.

[32] L. Redondo-Lpez, A. Prayati, J. L.-N. J. M.-O. and Garca-Hernando, A., *Problem Solving for Wireless Sensor Networks*. London: Springer-Verlag, 2008.

[33] Li, W. and Dai, H., "Distributed detection in wireless sensor networks using a multiple access channel," *IEEE Transactions on Signal Processing*, vol. 55, pp. 822–833, Mar. 2007.

[34] Lindsey, S. and C.S., R., "Pegasis: Power-efficient gathering in sensor information systems," IEEE Aerospace Conference, 2002.

[35] Lynch, J. and Loh, K., "A summary review of wireless sensors and sensor networks for structural health monitoring," *Shock and Vibration Digest*, vol. 38, pp. 91–130, Mar. 2006.

[36] Marshall, P., "Darpa connectionless networking program: Industry day briefing," tech. rep., 2003.

[37] Matolak, D. and Sun, R., "Air-ground channel characterization for unmanned aircraft systems: the hilly suburban environment," IEEE Vehicular Technology Conference, 2014.

[38] Matolak, D. and Sun, R., "Air-ground channel measurements and modeling for uas," *Aerospace and Electronic Systems Magazine*, vol. 29, pp. 30–35, Apr. 2014.

[39] Matolak, D. and Sun, R., "Initial results for air-ground channel measurements and modeling for unmanned aircraft systems: Over-sea," IEEE Aerospace Conference, 2014.

[40] Mengali, U., *Synchronization Techniques for Digital Receivers*. New York, NY: Springer, 1997.

[41] Mergen, G. and Tong, L., "Type based estimation over multiaccess channels," *IEEE Transactions on Signal Processing*, vol. 53, pp. 613–626, Feb. 2006.

[42] O. Younis, M. K. and Ramasubramanian, S., "Clustering in wireless sensor networks: recent developments and deployment challenges," *IEEE Network Magazine*, vol. 20, pp. 20–25, May 2006.

[43] Oh, N. and Lee, S., "Building a 2.4-ghz radio transceiver using ieee 802.15.4," *IEEE Circuits and Devices Magazine*, vol. 21, pp. 43–51, Jan. 2006.

[44] P. Braca, S. M. and Matta, V., "Single-transmission distributed detection via order statistics," *IEEE Transactions on Signal Processing*, vol. 60, pp. 2042–2048, Apr. 2012.

[45] Panasonic, "Pan4566 long range 802.15.4 transceiver," Wireless RF Module Electronics Components, Panasonic, 2009 [Online] Available:http://www.panasonic.com/industrial/components/modules/portal/ [Accessed: Aug. 4 2009].

[46] P.J. Chen, D.C. Rodger, S. S. M. H. and Tai, Y., "Microfabricated implantable parylene-based wireless passive intraocular pressure sensors," *Journal of Micro-electro-mechanical Systems*, vol. 17, pp. 1342–1351, Dec. 2008.

[47] Porat, B., *Digital Processing of Random Signals: Theory and Methods*. Englewood Cliffs, New Jersey: Prentice-Hall INC., 1993.

[48] Proakis, J., *Digital Communications*. New York, NY: McGraw-Hill Higher Education, 1998.

[49] Q. Cheng, P.K. Varshney, J. M. and Belcastro, C., "Distributed fault detection with correlated decision fusion," *IEEE Transactions on Aerospace and Electronic Systems*, vol. 45, pp. 1448–1465, Oct. 2009.

[50] Richards, M., *Fundamenals of Radar Signal Processing*. New York, NY: McGraw-Hill Higher Education, 2005.

[51] S. Marano, V. Matta, L. T. and Willett, P., "A likelihood-based multiple access for estimation in sensor networks," *IEEE Transactions on Signal Processing*, vol. 55, pp. 5155–5166, Nov. 2007.

[52] Scaglione, A. and Hong, Y. W., "Opportunistic large arrays: cooperative transmission in wireless multi-hop ad-hoc networks to reach far distances," *IEEE Transactions on Signal Proccessing*, vol. 51, pp. 2082–2092, Aug. 2003.

[53] Simon, M., "On the probability density function of the squared envelope of a sum of random phase vectors," *IEEE Transactions on Communications*, vol. 33, pp. 993–996, Sept. 1985.

[54] Sudevalayam, S. and Kulkarni, P., "Energy harvesting sensor nodes: Survey and implications," *IEEE Communications Surveys and Tutorials*, vol. 13, pp. 443–461, Sept. 2011.

[55] Suryadevara, N. and Mukhopadhyay, S., *Smart Homes: Design, Implementation and Issues*. Zurich, Switzerland: Springer International Publishing, 2015.

[56] T. Tachikawa, A. Oda, T. H. J. I. Y. W. and Nishi, H., "Cooperative distributed demand control by environmental sensor network-estimating the number of people by co 2 concentration," IEEE International Conference on Industrial Informatics, 2008.

[57] T. Yilmaz, R. F. and Hao, Y., "Detecting vital signs with wearable wireless sensors," *Sensors*, vol. 10, pp. 10837–10862, July 2010.

[58] TI, "Ti cc2420 manual," Low Power RF Protocols - Zigbee - CC2420, 2007. [Online] Available:http://focus.ti.com/docs/prod/folders/print/cc2420.html [Accessed: Aug. 10 2009].

[59] T.W. Hnat, E. Griffiths, R. D. and Whitehouse, K., "Doorjamb: unobtrusive room-level tracking of people in homes using doorway sensors," ACM Conference on Embedded Network Sensor Systems, 2012.

[60] W. Bajwa, J. Haupt, A. S. and Nowak, R., "Joint source-channel communication for distributed estimation in sensor network," *IEEE Transactions on Information Theory*, vol. 53, pp. 3629–3653, Oct. 2007.

[61] W. Heinzelman, A. C. and Balakrishnan, H., "Energy-efficient communication protocols for wireless microsensor networks," Hawaiian International Conference on Systems Science, 2000.

[62] Wimalajeewa, T. and Jayaweera, S., "Power efficient distributed estimation in a bandlimited wireless sensor network," Asilomar Conference on Signals, 2007.

[63] Y. J. Chang, H. Jung, S. C. and Weitnauer, M. A., "Network time synchronization for large multi-hop sensor networks using the cooperative analog-and-digital (candi) protocol," IEEE Wireless Communications and Networking Conference, 2014.

[64] Zheng, L. and Tse, D. N. C., "Diversity and multiplexing: A fundamental tradeoff in multipleantenna channels," *IEEE Transactions on Information Theory*, vol. 49, pp. 1073–1096, May 2003.

[65] Zhou, G. and Giannakis, G. B., "Harmonics in multiplicative and additive noise: performance analysis of cyclic estimators," *IEEE Transactions on Signal Processing*, vol. 43, pp. 1445–1460, June 1995.

VITA

Alper Akanser received his B.Sc. (with Highest Honors) in Electrical Engineering and M.Sc. in Electrical and Computer Engineering from Georgia Tech. His doctoral research was done under Dr. Mary Ann Weitnauer (formerly Mary Ann Ingram) on cooperative communications in wireless sensor networks. He currently works with Dr. Randall Guensler on various data collection projects at the Center for Transportation Operations and Safety at Georgia Tech. His current research interests include cooperative wireless communications, data fusion, transportation emissions simulation, and sidewalk quality estimation. He was previously an instructor in engineering at the Near East University, Cyprus. He has held industry positions at Usable Health in Atlanta, GA and Indeed in Austin, TX. He is a former Fulbright - Cyprus American Scholarship Program Scholar.